CAMBRIDGE
UNIVERSITY PRESS

Detrital zircon age and biostratigraphic and chemostratigraphic constraints on the Ediacaran–Cambrian transitional interval in the Irkutsk Cis–Sayans Uplift, southwestern Siberian Platform

Vasiliy V. Marusin[1,2] , Alena A. Kolesnikova[3], Boris B. Kochnev[1,2],
Nikolay B. Kuznetsov[3,4], Boris G. Pokrovsky[3], Tatiana V. Romanyuk[5],
Galina A. Karlova[1], Sergey V. Rud'ko[3,4], Andrey V. Shatsillo[4,5],
Alexander S. Dubenskiy[3], Victor S. Sheshukov[3] and Sergey M. Lyapunov[3]

[1]Department of Stratigraphy and Sedimentology, Trofimuk Institute of Petroleum Geology and Geophysics of SB RAS, Akademika Koptyuga Prospect 3, Novosibirsk 630090, Russia; [2]Department of Geology and Geophysics, Novosibirsk State University, Pirogova Street 1, Novosibirsk 630090, Russia; [3]Geological Institute of RAS, Pyzhevsky Lane 7, Moscow 119017, Russia; [4]Institute of the Earth's Crust of SB RAS, Lermontova Street 128, Irkutsk 664033, Russia and [5]Schmidt Institute of Physics of the Earth of RAS, Bol'shaya Gruzinskaya Street 10/1, Moscow 123995, Russia

Abstract

A number of ecological and geochemical transformations occurred during late Ediacaran and early Cambrian time, the effects of which are difficult to overestimate. However, the strong linkage of biostratigraphic and chemostratigraphic methods with lithofacies makes the localization of the Precambrian–Cambrian boundary and its correlation with lithologically contrasting sections highly debatable. We analyse the taxonomy and stratigraphic distribution of small skeletal fossils and trace fossils, the carbonate carbon and oxygen isotope composition, and U–Pb detrital zircon age in the Ediacaran–Cambrian transitional interval of the Irkutsk Cis–Sayans Uplift (southwestern Siberian Platform). This interval (Moty Group) comprises a transgressive succession with red-coloured alluvial to deltaic siliciclastic deposits (Shaman Formation) and overlying shallow-marine carbonates (Irkut Formation). The lower Irkut Formation hosts sporadic and poorly preserved tubular *Cambrotubulus* fossils, which are known from both the terminal Ediacaran Period (*c.* 550–541 Ma) and the Terreneuvian Epoch (541–521 Ma), and typical Fortunian trace fossils, including an index ichnotaxon of the Cambrian boundary *Treptichnus pedum*. The biostratigraphic and carbonate carbon isotope data and U–Pb concordia ages of 531.1 ± 5.2 Ma (mean weighted, 530.6 ± 5.3 Ma) of the five youngest zircon grains from the lower Irkut Formation indicate that at least the shallow-marine carbonates of the upper Moty Group correspond to the Cambrian Stage 2 (*c.* 529–521 Ma). In the Irkutsk Cis–Sayans Uplift, the Cambrian Period tentatively began before or during the accumulation of the alluvial to deltaic siliciclastic Khuzhir and Shaman formations, and this crucial divide remained unmarked in the palaeontological and isotopic records.

1. Introduction

The beginning of the Cambrian period was characterized by unprecedented ecological transformations and biodiversification rates that took place as a series of evolutionary events in the Ediacaran and Cambrian periods (e.g. Erwin & Valentine, 2013). Among others, these events are mirrored in the origin and further development of skeletal eumetazoans and ethologically (organism–sediment interaction style) diverse endobenthos (Mángano & Buatois, 2017; Wood *et al.* 2019) and in global changes in ocean-water phosphorus, carbon and oxygen cycling (e.g. Hantsoo *et al.* 2018; Lenton & Daines, 2018). Theoretically, the combination of these factors should cause the Precambrian–Cambrian boundary to be the easiest to localize in sedimentary successions. In contrast, the considerable facies dependence of available bio- and chemostratigraphic tools causes both the localization of this boundary and the correlation of lithologically contrasting sections to be highly speculative in practice (Rozanov *et al.* 1997; Landing *et al.* 2013; Babcock *et al.* 2014).

Trace fossils (Brasier *et al.* 1994; MacNaughton & Narbonne, 1999; Jensen, 2003) and, partially, acantomorphic acritarchs (Moczydłowska, 1991, 1998; Yao *et al.* 2005) serve well

for the stratigraphy of marine siliciclastic Ediacaran–Cambrian successions. However, the resolution of the latter is directly linked to specific taphonomic conditions (i.e. preservation in siltstones and mudstones). For carbonate-dominated successions in which the evolution of Ediacaran and early Cambrian endobenthic communities can barely be reconstructed because of ecological and taphonomic biases (Buatois, 2017), an informal group of small skeletal fossils (SSFs) (e.g. Khomentovsky & Karlova, 1993, 2002, 2005; Kouchinsky *et al.* 2012; Yang *et al.* 2014) and carbonate carbon isotope variations (Zhu *et al.* 2006, 2018; Maloof *et al.* 2010; Landing et al. 2013; Li *et al.* 2013) are used. However, correlations of the data that show the first appearance of specific ichnotaxa (*Treptichnus pedum*), SSF assemblage zones (*Anabarites trisulcatus – Protohertzina anabarica*) and negative $\delta^{13}C$ BACE (basal Cambrian carbon isotope excursion) values near the base of the Fortunian Stage remain subjects of strong debate (Rozanov *et al.* 1997; Peng *et al.* 2012; Landing *et al.* 2013; Babcock *et al.* 2014).

The Siberian Platform is one of the regions where this problem may be illustrated in detail. Highly diverse in lithology, the Ediacaran–Cambrian transitional strata of the Siberian Platform consist of intertidal and shelf successions that accumulated during eustatic sea-level rise (e.g. Peng *et al.* 2012) on underlying rocks of different ages (from Mesoproterozoic to late Ediacaran) (e.g. Sukhov *et al.* 2016). Composed primarily of epicontinental shallow-marine carbonates (Khomentovsky *et al.* 1972; Astashkin *et al.* 1991), the Ediacaran–Cambrian transitional strata of this region host diverse assemblages of small skeletal fauna (e.g. Rozanov *et al.* 1969; Khomentovsky & Karlova, 1993, 2002, 2005) and a representative carbon isotope record (e.g. Kaufman *et al.* 1996; Pelechaty *et al.* 1996; Kouchinsky *et al.* 2007; Kochnev *et al.* 2018). However, because marine siliciclastic and mixed carbonate-siliciclastic sections mostly occur to the NE of the Siberian Platform (Yudoma–Olenek facies region; Rozanov, 1992), the correlation of the carbonate successions of the central and western facies regions with worldwide Ediacaran–Cambrian sections is complicated.

Outside the Yudoma–Olenek facies region, mixed carbonate-siliciclastic successions of Ediacaran–Cambrian age are present along the southwestern margin of the Siberian Platform: the Yenisei Ridge and Cis–Sayans uplifts (Biryusa and Irkutsk). The latter two are also known as the 'Prisayan' uplifts (e.g. Priyatkina *et al.* 2018). All of these palaeobasins share similar sedimentological regimes in the upper Ediacaran and lower Cambrian strata: red-coloured continental and shallow-marine siliciclastic deposits that gradually change into lagoonal salt-bearing carbonates, ubiquitous within the southwestern Siberian Platform in the lower Cambrian strata (Khomentovsky *et al.* 1972; Melnikov *et al.* 2005; Sukhov *et al.* 2016; Sovetov, 2018). However, the limited occurrences of open-marine deposits between the continental and lagoonal facies within the intervals limit the application of biostratigraphic and chemostratigraphic methods. Hence, previous studies (Khomentovsky *et al.* 1998a; Kochnev & Karlova, 2010; Pokrovsky *et al.* 2012; Sovetov, 2018) have suggested the localization of the lower Fortunian boundary at the southwestern margin of the Siberian Platform based only on a regional correlation.

We report the first palaeontological data (e.g. trace fossils and SSFs), carbonate carbon and oxygen isotope compositions, and U–Pb detrital zircon ages of the Moty Group (Irkutsk Cis–Sayans Uplift; southwestern Siberian Platform). With no bio- or chemostratigraphic data available until now, traditional correlations of the Moty Group with the Ediacaran–Cambrian transitional interval by previous researchers were supported only

by its stratigraphic position between the Cryogenian–Ediacaran and Tommotian (Cambrian Stage 2) strata and by regional correlations (Khomentovsky *et al.* 1972; Sukhov *et al.* 2016; Sovetov, 2018). This interval consists of a mixed carbonate-siliciclastic succession that accumulated in continental and shallow-marine settings. Our data not only calibrate the age of the Moty Group, but also contribute to the chronology of the remarkable changes in sedimentation regimes that occurred along the southwestern margin of the Siberian Platform (in modern coordinates) during late Ediacaran and early Cambrian time.

2. Stratigraphy

In the Irkutsk Cis–Sayans Uplift (Fig. 1a, b), the Ediacaran–Cambrian transitional strata form a 700-m-thick carbonate-siliciclastic succession, which exhibits a gradual transition from mostly red-coloured coarse-grained sandstones and conglomerates to red-coloured cross-bedded medium- and coarse-grained sandstones and, higher in the section, a transition to fine crystalline dolostones, which are occasionally sand- and silt-enriched (Khomentovsky *et al.* 1972).

Although there is still no consensus on the stratigraphic subdivisions of this succession (Pisarchik, 1963; Khomentovsky *et al.* 1972; Krasnov *et al.* 1983; Sovetov, 2018), all interpretations disagree only on the nomenclature of the units rather than on the stratigraphic volumes or lithologies. We therefore use the version that was officially ratified by the USSR Interdepartmental Stratigraphic Committee (Krasnov *et al.* 1983): this succession includes the Moty Group, which includes the Khuzhir, Shaman and Irkut formations. The Moty Group unconformably overlaps the carbonate-siliciclastic Olkha Formation of early Ediacaran age, as is suggested by a regional correlation (Shenfil', 1991; Sovetov, 2018), and is capped by the salt-bearing carbonate Usol'e Formation of Tommotian age (Sukhov *et al.* 2016) (Fig. 1d). This unit of the Russian General Stratigraphic Chart *sensu lato* corresponds to Cambrian Stage 2 (Grazhdankin *et al.* 2020).

The Khuzhir Formation (35–76 m thick) is not exposed in the Irkutsk Cis–Sayans Uplift and is known only from the core of Borehole 2 (Khomentovsky *et al.* 1972) (Fig. 1b). This formation includes granule- and pebble-sized conglomerates in the basal part and the greenish-grey and reddish-brown middle- and coarse-grained sandstones above (Fig. 1d).

The Shaman Formation (320–380 m thick) conformably overlies the Khuzhir Formation. The Shaman Formation is composed primarily of red- and grey-coloured cross-bedded coarse-grained sandstones. The uppermost 30 m exhibits a gradual change of lithology to interbedded reddish-grey fine-grained sandstones and dark-red siltstones and mudstones. Early studies (Khomentovsky *et al.* 1972) documented individual 5-cm-thick interbeds of yellowish-grey dolostones in the uppermost Shaman Formation.

The dolostone-dominated Irkut Formation (130–250 m thick) overlies the Shaman Formation with a gradual transition. The lowermost 50 m of the Irkut Formation consists of interbedded wavy- and cross-bedded pinkish-grey medium- and fine-grained sandstones, red siltstones and grey sandy dolostones. The Irkut Formation is composed mostly of grey dolostones and silty dolostones with a silt content that increases towards the top of the formation (Fig. 1d).

In the Irkutsk Cis–Sayan Uplift, arguably the most well-exposed outcrop of the upper part of Shaman Formation and lower part of Irkut Formation, is located on the left bank of the Irkut River (37 km upstream from its mouth) on the Shaman Cliff
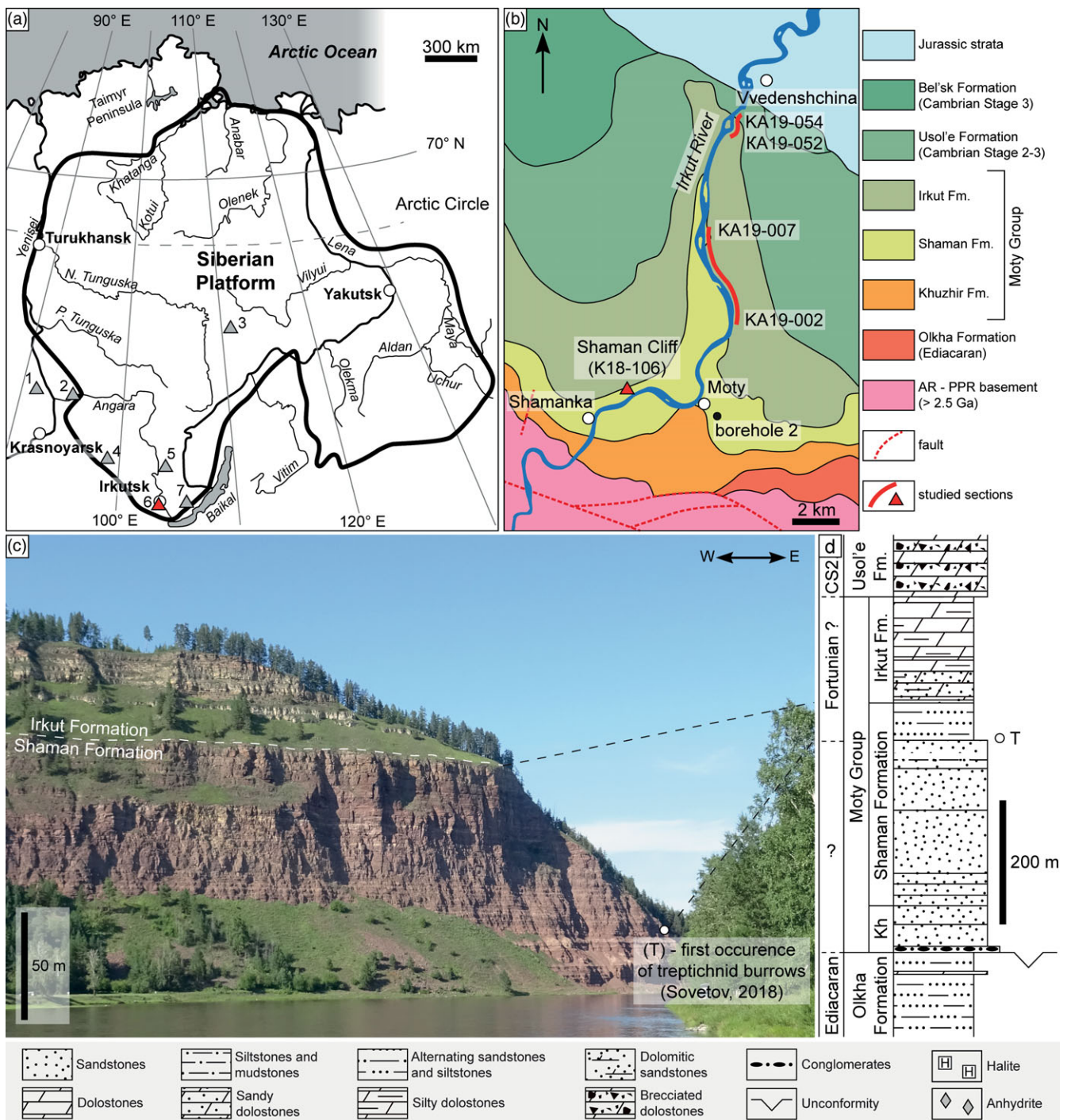
Fig. 1. (Colour online) Ediacaran–Cambrian transitional interval of the Irkutsk Cis–Sayans Uplift. (a) Sketch map of the Siberian Platform with the study area (red triangle) shown in detail in (b) and adjacent areas mentioned in the text: 1, eastern Fore-Yenisei Basin; 2, southern Yenisei Ridge; 3, central Siberian Platform; 4, Biryusa Cis–Sayans Uplift; 5, Irkutsk Amphitheatre; 6, Irkutsk Cis–Sayans Uplift; and 7, southwestern Cis–Baikal Region. (b) Simplified geological map with the studied sections of the upper Shaman, Irkut and lower Usol'e formations. (c) Boundary between the Shaman and Irkut formations (white dashed line) in the Shaman Cliff section (KA18-106). (d) Composite section of the Moty Group with previous age estimates (Krasnov *et al.* 1983; Sovetov, 2018). CS2 – Cambrian Stage 2; Kh – Khuzhir Formation; T – the lowest occurrence of sedimentary structures, documented and assigned to *Treptichnus pedum* by Sovetov (2018).

(section K18-106, 52° 05′ 05″ N, 103° 51′ 25″ E; Fig. 1b). The upper 110 m of the red-coloured Shaman Formation forms a very steep cliff that hinders its detailed lithological study and sampling potential (Fig. 1c). These strata are composed of planar-laminated granule-sized conglomerates and middle- to coarse-grained sandstones with tabular and trough cross-bedding (Fig. 2b). The bedding surfaces commonly show wave and current ripple marks and large desiccation cracks (Fig. 2a). The uppermost 45 m of the Shaman Formation consists of reddish-grey trough cross-bedded and planar-laminated medium-grained sandstones interbedded with reddish- and yellowish-grey siltstones and mudstones.
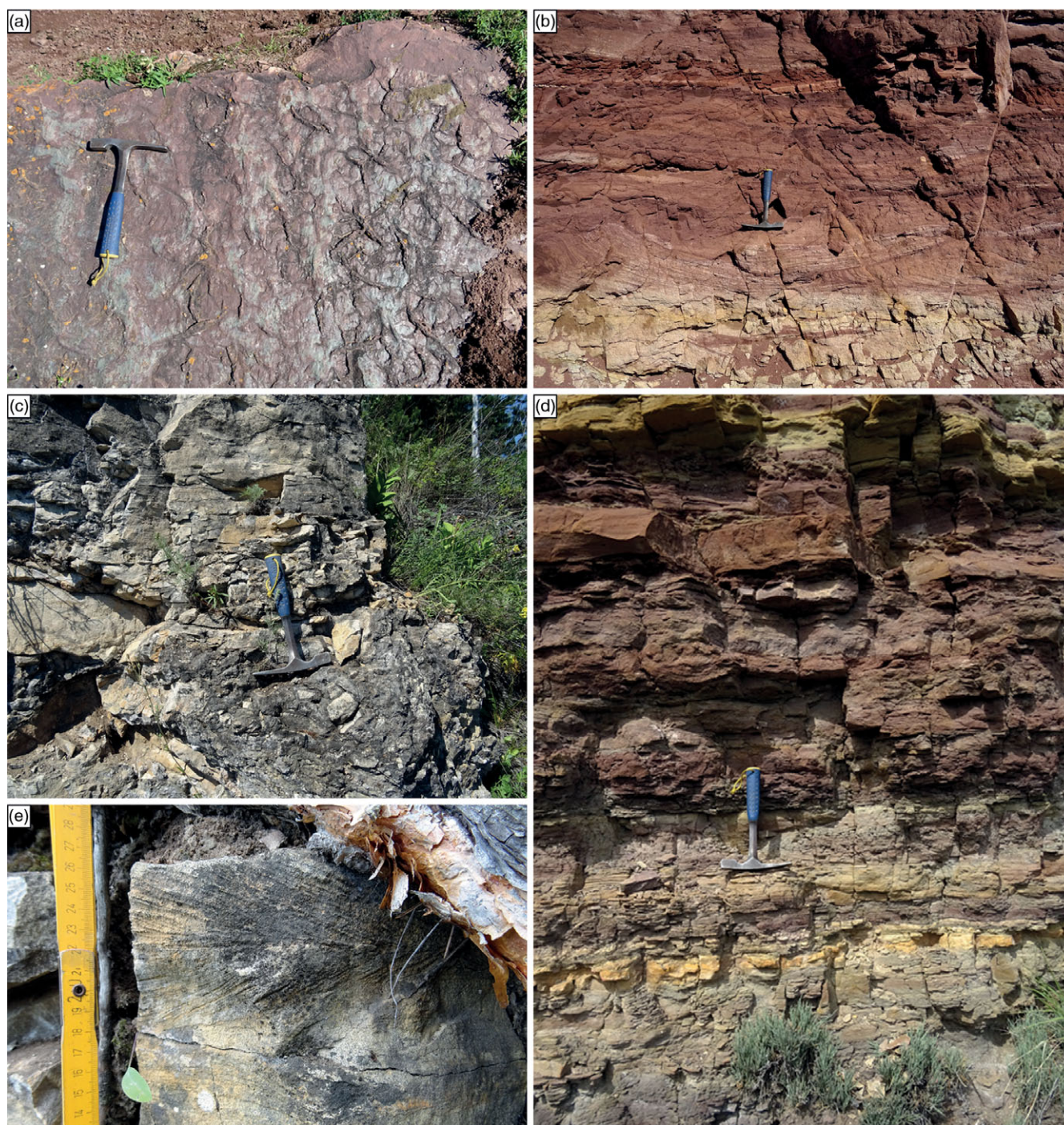
Fig. 2. (Colour online) Lithology of the upper Shaman and lower Irkut formations. (a) Sand-filled desiccation cracks and large symmetrical ripple marks on the top of coarse-grained sandstones (upper Shaman Formation, *c.* 100 m below the top). (b) Red trough cross-bedded coarse-grained sandstones (upper Shaman Formation, *c.* 100 m below the top). (c) Interbed of collapse breccias in dolostones of the lower Irkut Formation (12 m above the base). (d) Alternating reddish-grey and yellowish-grey dolomitic siltstones and mudstones and dolomitic sandstones with planar laminations and wavy and trough cross-bedding with thin interbeds of yellowish-grey sandy dolostones (lower Irkut Formation, 26 m above the base). (e) Dolomitic sandstones with herringbone cross-stratification (lower Irkut Formation, 30 m above the base). Length of the hammer: 28 cm.

In the Shaman Cliff, there is a 1-m-thick bed of light-grey coarse-grained quartz sandstone at the very base of the Irkut Formation. This layer is overlain by a poorly exposed interval (11 m) with pinkish-grey and grey middle- to-fine-grained sandstones, siltstones, mudstones and silty dolostones, which are documented in small individual outcrops (Fig. 1c). The overlying 45 m of this unit is composed of yellowish-grey and grey massive and finely laminated dolostones interbedded with pinkish-grey and grey sandy dolostones and dolomitic sandstones and siltstones (Fig. 2d). The sandstones exhibit planar laminations and small-scale (up to 5 cm thick) hummocky, trough and herringbone cross-bedding (Fig. 2d, e), and often carry symmetric and asymmetric ripple marks. The lower part of this interval includes a single 1-m-thick bed of brecciated dolostone (Fig. 2c). Downstream along

the Irkut River, the upper Irkut Formation crops out as a series of natural exposures on its right bank (KA19-002–KA19-007: 52° 06′ 20″ N, 103° 55′ 00″ E to 52° 09′ 00″ N, 103° 54′ 05″ E; KA19-052, 52° 11′ 05″ N, 103° 55′ 15″ E) up to the brecciated cavernous dolostones of the overlying Usol'e Formation (KA19-054: 52° 11′ 20″ N, 103° 55′ 35″ E; Fig. 1b). In these sections, the Irkut Formation is composed of interbedded massive dolostones and finely laminated silty dolostones with a gradual increase in the silt content upwards. The uppermost 50 m of the Irkut Formation is only sporadically exposed in several isolated outcrops.

As noted by previous authors (e.g. Khomentovsky *et al.* 1972; Sukhov *et al.* 2016), the base of the salt-bearing Usol'e Formation is marked by the first occurrence and further development of cavernous brecciated dolostones above the silty dolostones of the Irkut Formation. However, our field observations reveal that this change in lithology is gradual.

Considering the lithologies and regional correlations of the Moty Group with its stratigraphic analogues in the southern Yenisei Ridge (e.g. Redkolesnaya and Ostrovnoy Formations) and Biryusa Cis–Sayans Uplift (e.g. Ust'–Tagul Formation) (Fig. 3), the Moty Group represents a transgressive sequence with a gradual change from alluvial to deltaic depositional systems (lower Shaman Formation) to shallow-marine environments (e.g. upper Shaman and Irkut formations) and a parallel decrease in siliciclastic influx into the basin (Sovetov, 1977, 2018). At the same time, the typical shallow-marine sedimentary structures in the Irkut Formation (trough and herringbone cross-bedding, and wave ripple marks) and the following rapid change into the evaporitic, salt-bearing facies of the Usol'e Formation (Sukhov *et al.* 2016) suggest accumulation of the Irkut Formation in intertidal and shoreface zones.

With no robust bio- or chemostratigraphic data available, the Ediacaran–Cambrian age of the Moty Group has long been estimated based only on regional correlation data (Khomentovsky *et al.* 1972; Shenfil', 1991; Sukhov *et al.* 2016) (Fig. 3). In 2018, JK Sovetov reported the first occurrence of *Treptichnus pedum* 60 m below the top of the Shaman Formation (Sovetov, 2018, fig. 3a; Fig. 1c, d). The correlation of the upper Shaman and Irkut formations with the middle Ust'–Tagul Formation (Biryusa Cis–Sayans Uplift), which exhibit generally similar lithologies and bear *T. pedum* (Kochnev & Karlova, 2010; Sovetov & Jensen, 2010), provided evidence for associating these units with the Cambrian Fortunian Stage (Sovetov, 2018). The youngest detrital zircon U–Pb ages of 886 ± 6 Ma from the Ust'–Tagul Formation and 586 ± 20 Ma and 589 ± 33 Ma from the Redkolesnaya Formation of the southern Yenisei Ridge (Priyatkina *et al.* 2018) provide some information regarding the age of the Moty Group. In this publication, the authors also note unspecified '~542-534 Ma fossils' from the Redkolesnaya Formation by referring to Liu *et al.* (2013). However, when considering all known reports of fossil occurrences from this unit (Chechel', 1976; Liu *et al.* 2013), only discoidal *Cyclomedusa* are present, which is typical for the late Ediacaran Period.

Considering the data from the southwestern Cis–Baikal Region, the U–Pb ages of 554 ± 12 Ma for the seven youngest concordant detrital zircon grains from the Ushakovka Formation (Gladkochub *et al.* 2013) suggest a late Ediacaran age for this unit and its stratigraphic analogue in the Irkutsk Cis–Sayans Uplift – lower Moty Group (Khuzhir and lower Shaman formations) (Sovetov, 2018). As noted by Gladkochub *et al.* (2013), the Ushakovka sandstones also contain individual Cambrian detrital zircons (534 ± 14 and 534 ± 16 Ma). We agree with the authors that the scarcity of

Cambrian zircons (only two grains were registered) rejects their use as an indicator of the maximum depositional age estimate.

The Fortunian age (541–529 Ma) of the upper Moty Group can also be indirectly inferred by correlation of the overlying Usol'e Formation with the Cambrian Stage 2 (Tommotian Stage; Krasnov *et al.* 1983; Sukhov *et al.* 2016). This age is based on a comparison of carbon isotope data from the Ediacaran–Cambrian strata of the Irkutsk Amphitheatre (Vinogradov *et al.* 2006) with the Tommotian stratotype (Aldan River; Brasier *et al.* 1993). This assumption is also supported by the skeletal fossil occurrence in the basal Tommotian *Nochoroicyathus sunnaginicus* Assemblage Zone in the Usol'e Formation of the eastern Fore–Yenisei sedimentary basin (Averinskaya-150 borehole; Khomentovsky & Karlova, 2005) and in its analogue in the central Siberian Platform (Bilir Formation; Sukhov *et al.* 2016) (Fig. 3). The underlying strata (e.g. Tetere and Yuryakh formations) host skeletal fossils of the uppermost Fortunian *Purella antiqua* Assemblage Zone (Khomentovsky *et al.* 1998b; Grazhdankin *et al.* 2015). However, recent bio- and chemostratigraphic data from the Ediacaran–Cambrian transitional interval of the central Siberian Platform suggest that, at least in some sections, the lower Cambrian Stage 2 boundary is located as low as 100 m below the Usol'e–Bilir Formation (Kochnev *et al.* 2018).

3. Materials and methods

As noted in the previous section, the upper Shaman Formation is exposed as a 110-m-high cliff in the Shaman Cliff section (Fig. 1c). Its lithological study and sampling are therefore not possible without specialized rock-climbing equipment, except for the lowermost few metres accessible from below. The uppermost 11 m of the Shaman Formation were logged and sampled in the outcrops exposed downstream along the Irkut River between Moty and Vvedenshchina villages (KA19-002–KA19-054 in Fig. 1b). Our study focuses mostly on the Irkut Formation and the lowermost 27 m of the Usol'e Formation, which are documented in the upper part of the Shaman Cliff (lower 45 m of the Irkut Formation) and in the exposures along the Irkut River (see Section 2 for coordinates; Fig. 1b). Precise section logging was accompanied by sampling for further SSF extractions (25 samples) and carbon and oxygen isotope studies (59 samples from the Irkut Formation and six from the Usol'e Formation). For carbon and oxygen isotope analyses, those intervals with lesser degrees of diagenetic alteration were preferentially collected, which determined the overall sampling density (online Supplementary Table S1, available at http://journals.cambridge.org/geo). The macroscopic sampling criteria included a micritic composition or minimal recrystallization of the carbonates, the presence of laminations or their relics, and a lack of structural heterogeneity (inclusions or evidence of dissolution). All the SSFs further discussed are stored at the Trofimuk Institute of Petroleum Geology and Geophysics of SB RAS (IPGG SB RAS), Novosibirsk.

All images of macroscopic objects (e.g. sedimentary structures and slabs with ichnofossils) presented here were obtained with a digital camera during fieldwork in the Irkutsk Cis–Sayans Uplift in 2017 and 2019. Initial ichnotaxonomic identification of the trace fossils was performed during the fieldwork and was further updated with the morphometric parameters derived by examining the images and collected specimens, which are stored at the Geological Institute of RAS (GIN RAS), Moscow.

Small skeletal fossils were extracted from the dolostone samples in IPGG SB RAS by applying a technique of gentle rock-dissolution in 2% buffered acetic acid (see Marusin *et al.* 2019 for details of the
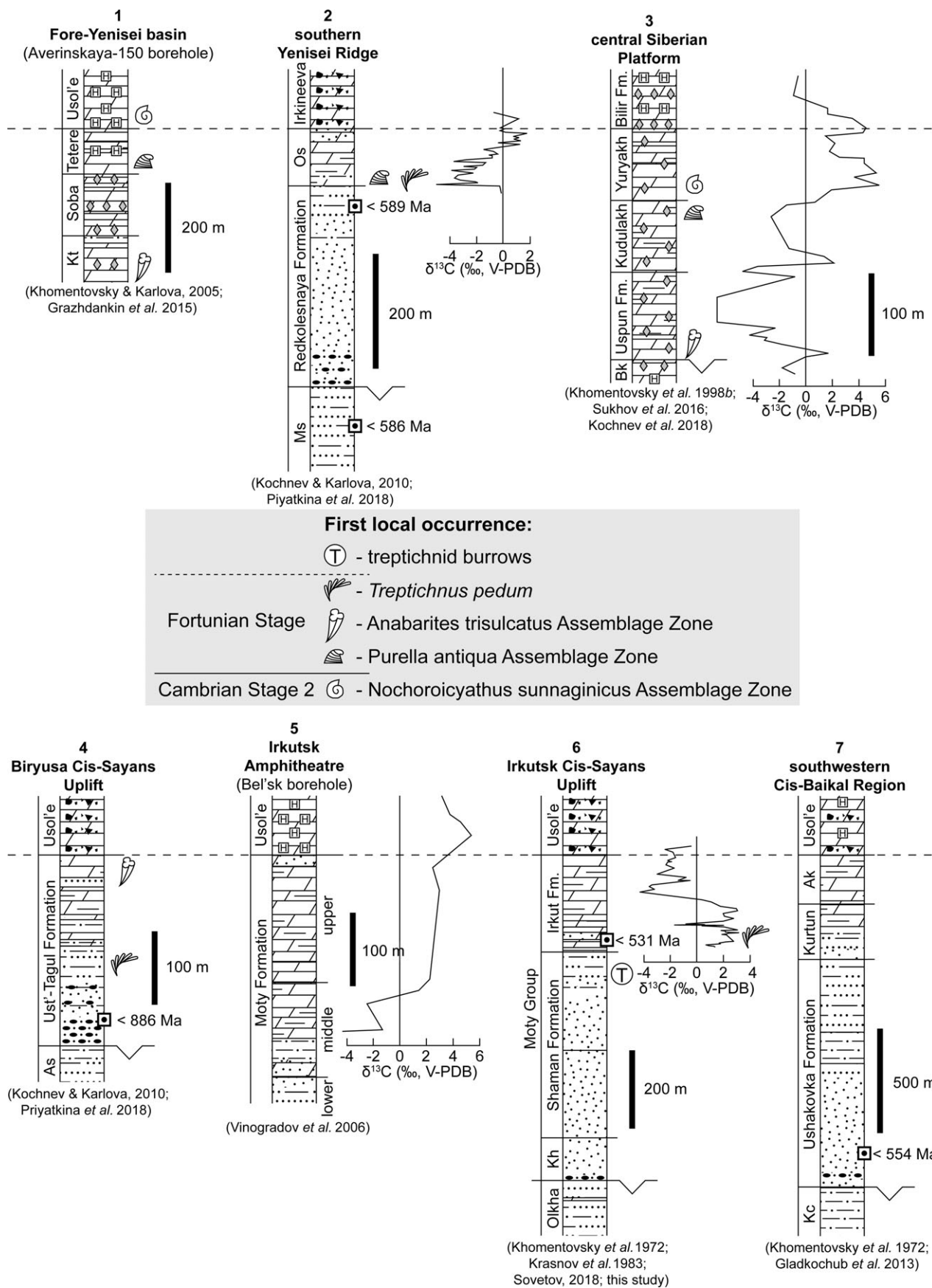
Fig. 3. Ediacaran–Cambrian transitional strata of the southwestern Siberian Platform and eastern Fore–Yenisei Basin (Fig. 1a) and their age constraints. The horizontal dashed line marks the base of salt-bearing carbonate formations, which are commonly used as the regional marker horizon in stratigraphic schemes (e.g. Krasnov et al. 1983). Ak – Ayankan; As – Aisa; Bk – Byuk; Kc – Kochergat; Kh – Khuzhir; Kt – Katanga; Ms – Moshakovka; Os – Ostrovnoy. Lithologies correspond to the key in Figure 1.

method). The dry residual materials were studied under a Carl Zeiss Stemi 2000 (6.5–50× magnification) stereomicroscope for fossil extractions. Scanning electron microscopy (SEM) of the small skeletal fossils was performed with a Tescan MIRA 3, and the samples were stored at the Analytical Center for Multielemental and Isotope Research (IGM SB RAS, Novosibirsk). Prior to analysis, the fossils were mounted on aluminium stubs and were coated with chrome and carbon.

Carbon (δ^{13}C) and oxygen (δ^{18}O) analyses of the carbonates were carried out at the GIN RAS (Moscow) using a Finnigan Delta-V (Thermo Electron Corp.) mass spectrometer equipped with a Gas Bench-II line. Prior to the analyses, powder was drilled from the most lithologically homogenous zones of the samples. Depending on the carbonate amount, 0.5–1.5 mg of the powder was dissolved in orthophosphoric acid at 50°C. The δ^{13}C and δ^{18}O values are given in per mille (‰) units relative to the international V-PDB (Vienna Pee Dee Belemnite) and V-SMOW (Vienna Standard Mean Ocean Water) standards, respectively. The analytical accuracies of the carbon and oxygen isotope measurements are within ±0.1‰ and ±0.2‰, respectively, and were controlled by external standards and calibrated by the NBS-19 international standard (Friedman *et al.* 1982). To evaluate diagenetic alteration, we applied δ^{18}O values and paired correlations of δ^{13}C and δ^{18}O (Kaufman & Knoll, 1995). Oxygen isotope values below 20‰ V-SMOW (or < −10‰ V-PDB) and/or direct correlation of δ^{13}C and δ^{18}O indicated considerable post-sedimentary alteration. Such samples from the Moty Group (11 samples) were therefore excluded from further discussion (online Supplementary Table S1).

The field study did not include specific sampling of any material for extraction and U–Pb dating of detrital zircons. The detrital zircon grains were extracted from a slab of sandy dolostones (sample K18-106) collected 28 m above the base of the Irkut Formation in the Shaman Cliff. The sample consists of a 1-cm-thick slab (1.5 kg total weight) with numerous trace fossils in positive hyporelief. The sample was originally collected as a palaeontological sample, but also revealed abundant detrital zircons in thin sections. The sample was crushed to *c.* 1-cm-sized clasts and disintegrated in 1 N hydrochloric acid at room temperature. The residual materials were levigated and sifted with a 50 μm sieve under water flow. The dried material was separated with a low-viscosity aqueous sodium heteropolyoxotungstate heavy liquid (HSP-W, density 2.85 ± 0.05 g cm⁻³) to extract the heavy mineral fractions. After a magnetic separation procedure, 186 zircon grains were handpicked from the non-magnetic fraction under a binocular microscope. They were mounted in epoxy resin and polished. For each grain, 5–6 optical slices were made with plane-polarized light under a stereo binocular microscope to localize areas (at least 25 μm in diameter) with no visible inclusions, cracks or metamict zones for analysis. Images of the high-relief objects were obtained by stacking the individual optical slices with Helicon Focus software. Immediately before analysis, the epoxy mount with zircons was washed in an ultrasonic bath filled with 5% nitric acid, rinsed with distilled water, and dried at room temperature.

Laser ablation (LA) -inductively coupled plasma mass spectrometry (ICP-MS) analyses of detrital zircon grains (dZr) were performed at the GIN RAS using an Element2 (Thermo Scientific) ICP-MS coupled with a NWR-213 (Electro Scientific) laser ablation system (Nikishin *et al.* 2020) and configured to a spot size 25 μm in diameter. Helium gas was used as the laser ablation carrier with a further admixture of argon. Precise filtration and gas blending were applied to reduce gas noise and increase the stability of the analytical signal. The zircon standard GJ-1 (Jackson *et al.*

2004; Elhlou *et al.* 2006), which was provided by the ARC National Key Center for Geochemical Evolution and Metallogeny of Continents (GEMOC), Macquarie University (Sydney, Australia), with a ^{206}Pb/^{238}U age of 601.9 ± 0.4 Ma (Horstwood *et al.* 2016), was used as the primary standard for data reduction. The zircon standards 91500 (Wiedenbeck *et al.* 1995, 2004; Yuan *et al.* 2008) and Plesovice (Sláma *et al.* 2008) were measured as secondary standards for accuracy evaluations. These two standards provided weighted ^{206}Pb/^{238}U concordia ages (2σ) of 1068 ± 6 Ma (91500; n = 15) and 338 ± 2 Ma (Plesovice; n = 14), which were positively correlated with the verified CA-ID-TIMS ^{206}Pb/^{238}U ages of 1063.5 ± 0.4 Ma and 337.2 ± 0.1 Ma, respectively (Horstwood *et al.* 2016). The primary analytical data were processed through GLITTER (Griffin *et al.* 2008), ISOPLOT (Ludwig *et al.* 2012) and AgePick (Gehrels, 2012) software, and applied the methods and constants given in Romanyuk *et al.* (2018). The ^{207}Pb/^{235}U ratios were calculated from the ^{206}Pb/^{238}U and ^{207}Pb/^{206}Pb ratios assuming that ^{238}U/^{235}U = 137.88. In online Supplementary Table S2 (available at http://journals.cambridge.org/geo), all errors were within a 2σ interval. Relative probability density (RPD) diagrams of the ages of the analysed samples were plotted using ^{206}Pb/^{238}U for grains younger than 1.2 Ga and ^{207}Pb/^{206}Pb for those older than 1.2 Ga (e.g. Gehrels *et al.* 2008). In the studied samples, we sorted out grains that exceeded the cut-off criteria of discordance (D) of −5 ≤ D ≤ 10: D_1 (^{207}Pb/^{235}U versus ^{206}Pb/^{238}U) for the grains younger than 1.2 Ga and D_2 (^{207}Pb/^{206}Pb versus ^{206}Pb/^{238}U) for the grains older than 1.2 Ga (e.g. Nemchin & Cawood, 2005). To evaluate the maximum depositional ages, we applied a conservative estimate (Dickinson & Gehrels, 2009) based on a concordia age from a group of the youngest grains (n = 5) with |D_{1and2}| < 5 (online Supplementary Table S2).

4. Results

4.a. Trace fossils

Trace fossils first occur in the studied sections of the Moty Group at 28 m above the base of the Irkut Formation and in the overlying 20 m of this unit. These fossils are associated exclusively with interbeds of grey sandy dolostones and pinkish-grey dolomitic sandstones, and appear there in positive hyporelief or negative epirelief; they are rarely seen in full relief. In the overlying strata, trace fossils were not documented.

Horizontal burrows dominate in the ichnoassemblage of the Irkut Formation. Most of those are composed of morphologically simple subhorizontal, straight and gently curved *Palaeophycus tubularis* (4–8 mm in diameter) with no surface ornamentation, and are filled with sediment that is similar to the host rock (Fig. 4b, c). On some bedding surfaces, *Palaeophycus* demonstrate high densities and commonly overlap each other. The sporadic occurrence of dichotomous Y- and T-shaped branching in these burrows suggests that a producer may have used them several times. However, the lack of complex branching patterns and associated vertical shafts in the studied material does not support interpretation of any of these trace fossils as network burrows (e.g. *Thalassinoides*).

Horizontal probing burrows, which were assigned to *Treptichnus pedum* (up to 3 mm in diameter), first occur 28 m above the base of the Irkut Formation and are common in the ichnoassemblage. These fossils mostly occur in positive hyporelief (Fig. 4e) but are also documented in negative epirelief on bedding
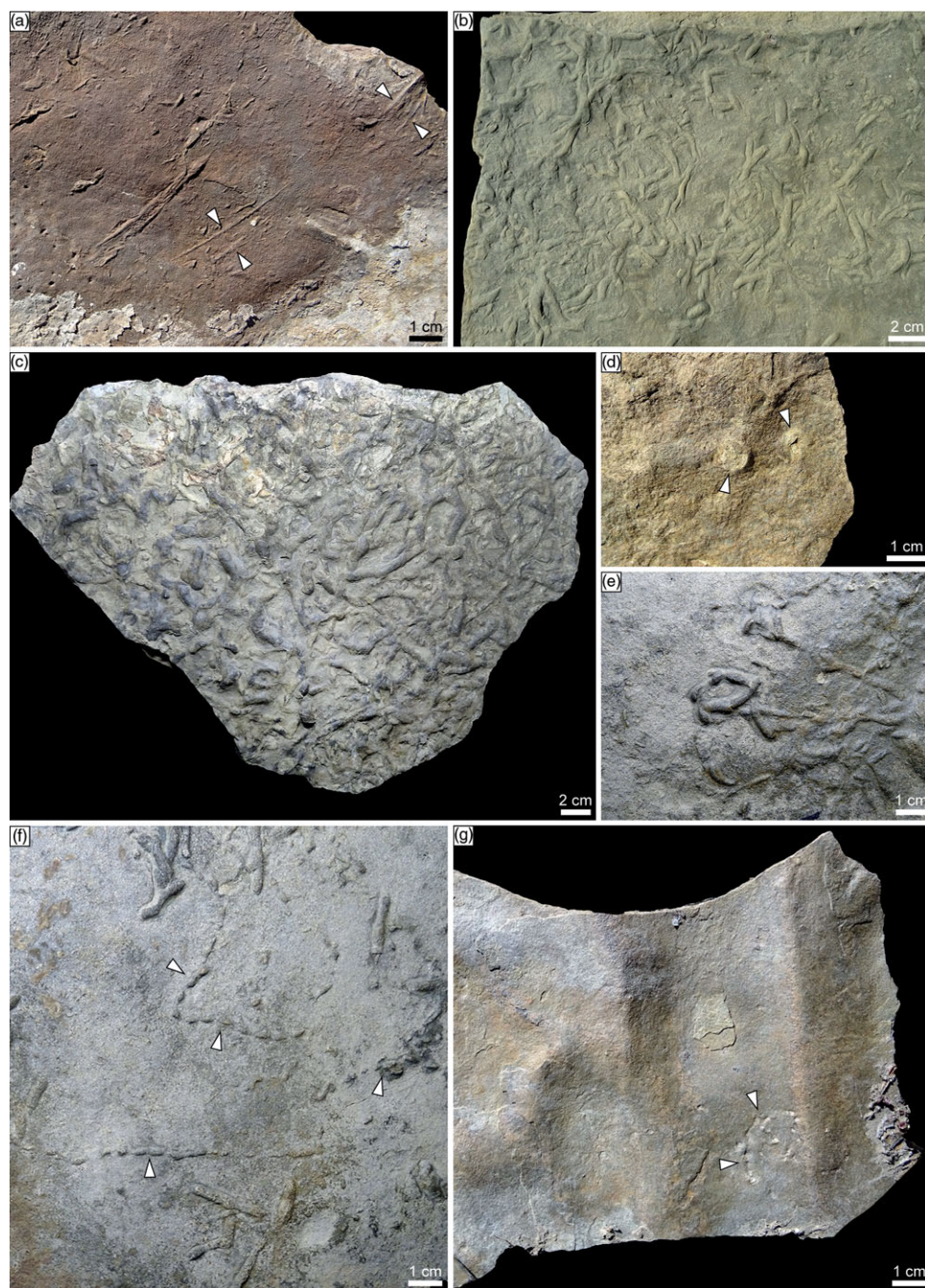
Fig. 4. (Colour online) Trace fossils from the lower Irkut Formation. (a) Parallel scratches *Monomorphichnus* isp. (white arrows) in positive hyporelief on the bedding surface of reddish-grey dolomitic sandstones. Numerous (b) low- and (c) high-relief subhorizontal *Palaeophycus tubularis* in positive hyporelief in grey sandy dolostones. (d) Bedding-parallel sections of subvertical cylindrical *Skolithos* in yellowish-grey sandy dolostones. (e) Positive hyporelief *Treptichnus pedum* in grey sandy dolostones. (f) Aligned series of short low-relief projections in positive hyporelief (white arrows), which are assigned to *Treptichnus* isp. in grey sandy dolostones. (g) Series of vertical probes *Treptichnus* isp. in negative epirelief (white arrows) and parallel symmetrical wave ripple marks on the top of grey sandy dolostones.

surfaces with symmetrical wave ripple marks (Fig. 4g). In some cases, they are found together with aligned series of isolated elliptical and circular segments of similar diameter (Fig. 4f), and exhibit similar morphology to those documented earlier from the upper Shaman Formation (Sovetov, 2018, fig. 3a). Although such a morphology is typical for treptichnids, the lack of ichnospecific features (e.g. short segments joining each other from the same side at low angles near the centre) challenges the original identification of these structures from the Shaman Formation as *Treptichnus pedum* (Sovetov, 2018). We therefore assigned these burrows from the Shaman and Irkut formations to *Treptichnus* isp.

The bedding planes occasionally carry series of thin parallel ridges in positive hyporelief (Fig. 4a). These structures may be tool marks. However, paired parallel occurrences and the equal or close

depths of these structures are typical morphological elements of arthropod-produced scratches *Monomorphichnus* isp., which have been widely documented in the Fortunian and younger strata (e.g. Mángano & Buatois, 2014). The lower Irkut Formation hosts only sporadic and poorly preserved vertical burrows. They appear only as isolated, low-relief, circular structures (5–7 mm in diameter) on bedding planes, and are filled with sediment that is lighter than the host rock (Fig. 4d). Although no vertical shafts were documented on the bedding-normal surfaces, these structures share a similar morphology with the bedding-parallel sections of the simple cylindrical subvertical burrows of *Skolithos* (e.g. Walter *et al.* 1989, fig. 15D; Jensen, 1997, fig. 5A); we therefore provisionally assigned these structures to *Skolithos* isp. However, further detailed study is necessary to verify this interpretation.
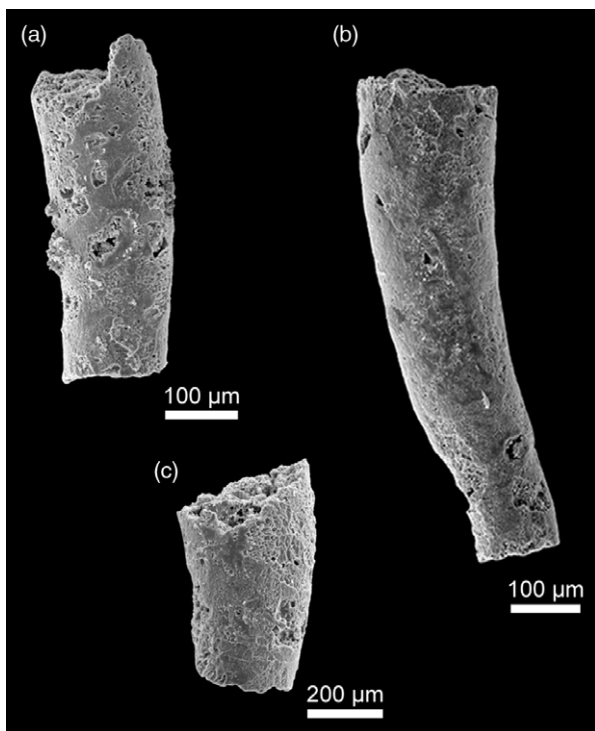
Fig. 5. SEM images of inner-mould fragments of conical shells assigned to *Cambrotubulus* sp. from the lower Irkut Formation (*c.* 30 m above the base): specimens (a) KM17-2/19-1, (b) KM17-2/19-3 and (c) KM17-2/19-4.

Field observations and laboratory studies of the sampled material revealed that the horizontal and rare vertical burrows had a minimal impact on the sedimentary structures. Bioturbation affected only thin (1–2 cm) intervals of the layers.

4.b. Small skeletal fossils

The Moty Group and lower Usol'e Formation are poorly characterized by small skeletal fossils. After dissolution of all of the specifically sampled material, individual skeletal fossils were documented only in two samples of dolomitic sandstones that were collected at 29.2 m and 31 m above the base of the Irkut Formation. These fossils consist of poorly preserved fragments (up to 700 μm long and up to 200 μm in diameter) of straight and gently curved conical inner moulds with circular cross-sections (Fig. 5). The moulds are smooth, carry no relics of mineralized shells and are composed of micritic dolostone. These fragments do not exhibit any specific morphology (e.g. cone-in-cone structures or triradial symmetry) and therefore correspond to simple tubular *Cambrotubulus*, which are abundant in the terminal Ediacaran and Fortunian strata (e.g. Nagovitsin *et al.* 2015).

4.c. Carbonate carbon and oxygen isotope systems

The carbon and oxygen isotope data derived from 11 samples from three intervals in the lower Irkut Formation exhibit significant diagenetic alteration, as is seen in the correlations between the $\delta^{13}C$ and $\delta^{18}O$ values (online Supplementary Table S1). Although high Pearson correlation coefficients (R of 0.99 for the samples from 30.3 to 33.5 m above the formation base) are not representative for such small numbers of samples in each group, the correlated carbon and oxygen isotope values for each of these three groups dramatically increased the overall C–O correlations

(ranging from 0.34 to 0.69; online Supplementary Table S1). Only by excluding all three groups, the R coefficient reaches 0.13 and does not exceed the critical correlation value of $R = 0.21$ (Fisher & Yates, 1974). When considered separately from the other criteria, the covariations of the carbon and oxygen isotope values do not necessarily reflect diagenetic alteration of the studied material. However, all samples from the lower Irkut Formation with high correlation coefficients (Fig. 6) consist of sandy dolostones and dolomitic sandstones and include those with very low $\delta^{18}O$ values (below 20‰ V-SMOW), which indicates post-sedimentary alteration (online Supplementary Table S1). We therefore excluded these data from further discussion (Fig. 6).

Dolostones in the lower 100 m of the Irkut Formation demonstrate strongly positive $\delta^{13}C$ values from 0.5‰ to 3.1‰ from a single interval in the middle, where the carbon isotope ratios oscillate between –1.7‰ and 2.1‰ (Fig. 6). This interval technically splits the positive $\delta^{13}C$ plateau in the lower Irkut Formation into two individual excursions. However, since it includes only several layers (5.5 m in total) and the carbon isotope values oscillate irregularly there, we assume that this minor isotope shift was caused by local conditions rather than mirroring the global short-period changes in seawater isotope compositions. In the same part of the section, the oxygen isotope values vary irregularly between 23‰ and 28.7‰ with a single short decrease down to 21.1‰ at 49.5 m above the base. In contrast, the upper Irkut (*c.* 70 m) and lower Usol'e (26.5 m) formations show negative $\delta^{13}C$ values from –4.3‰ to –0.4‰ and stable $\delta^{18}O$ values remaining at 25.2‰ to 26.4‰. The lack of any sharp shifts in the carbon and oxygen isotope compositions at the Irkut–Usol'e transitional interval indirectly supports an earlier suggestion regarding the absence of any measurable depositional hiatus between these two formations (Fig. 6).

4.d. Detrital zircon geochronology

In the studied sample K18-106 (28 m above the base of the Irkut Formation), U–Pb ages were derived for 149 detrital zircon grains (online Supplementary Table S2). These ages are based on three ratios ($^{206}Pb/^{238}U$, $^{207}Pb/^{206}Pb$ and $^{207}Pb/^{235}U$) that were measured and calculated for each grain. The integrated results are shown on the concordia diagram (Fig. 7a–c). Applying the discordance criteria mentioned in Section 3 resulted in the exclusion of 50 grains from further consideration. Hence, the histograms and age spectra (Fig. 7d, e) are based on 99 grains that were suitable for interpretation. Application of even more stringent parameters $|D_{1\ or\ 2}| < 5$ notably affects only the quantity of zircon selection (49 dZr versus the 99 grains we used), but does not significantly change the age estimates.

Among the concordant grains, all U–Pb ages lie between 481 ± 10 Ma ($D_1 = 7.5\%$) and 3237 ± 26 Ma ($D_2 = 0.1\%$) (online Supplementary Table S2). All ages fall into four groups (Fig. 7d). The largest group (Z2) of late Neoproterozoic – early Cambrian age includes 88 dZr: 86 grains with ages ranging from 663 ± 24 Ma ($D_1 = 2.6\%$) to 522 ± 12 Ma ($D_1 = 3.1\%$), and 2 grains with ages of 702 ± 16 Ma ($D_1 = 3.0\%$) and 771 ± 16 Ma ($D = 0.5\%$). These zircons represent 89% of the total sample population and therefore form a 'dominant' group (Andersen, 2005). Within this group, the zircon ages consist of four minor peaks seen on the RPD diagram (Fig. 7e) with maxima at 535 Ma (28 dZr), 550 Ma (28 dZr), 576 Ma (17 dZr) and 634 Ma (11 dZr). All of the other age groups (e.g. Z1, Z3 and Z4) are scant ('accessory', in the usage of Andersen, 2005), and each of them consists of no more than 5% of the total grain quantity. The Z1 group consists of only two grains
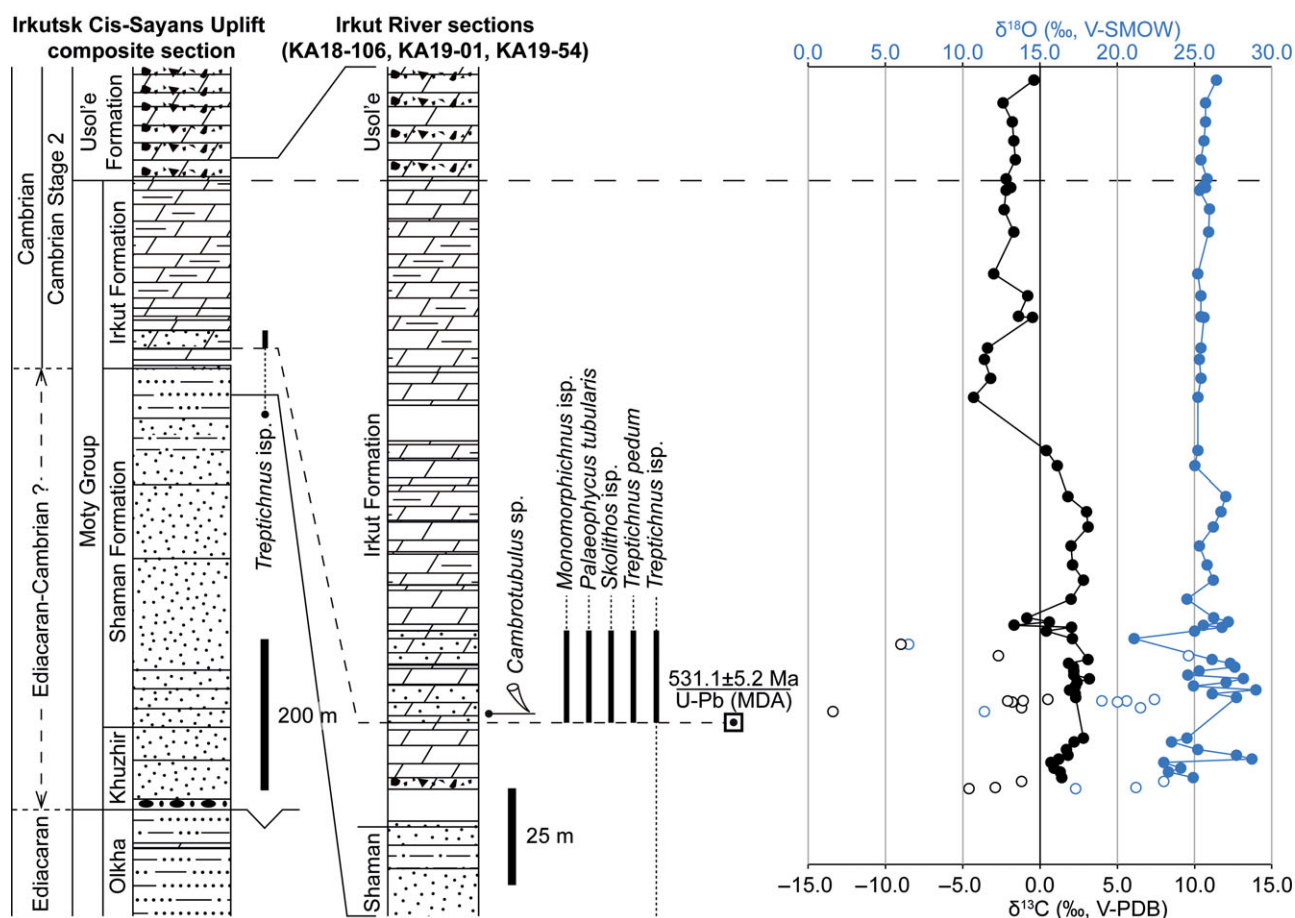
Fig. 6. (Colour online) Age constraints of the Ediacaran–Cambrian transitional interval of the Irkutsk Cis–Sayans Uplift, as shown by distribution of trace fossils, small skeletal fossils, carbonate carbon and oxygen isotope variations (online Supplementary Table S1) and U–Pb detrital zircon ages (concordia age; weighted mean, 530.6 ± 5.3 Ma) (Fig. 7). MDA – maximum depositional age. Lithologies correspond to the key in Figure 1.

(2% of the total dZr) with close but statistically irrelevant ages of 481 ± 10 Ma (D_1 = 7.5%) and 509 ± 12 Ma (D_1 = 6.1%). Four zircons (4% of the total dZr) with late Palaeoproterozoic ages between 1974 ± 14 Ma (D_2 = –3.2%) and 1809 ± 18 Ma (D_2 = –2.0%) comprise age group Z3. Age group Z4 includes five zircons (5% of the total dZr) with Archaean ages between 3237 ± 13 Ma (D_2 = 0.1%) and 2741 ± 14 Ma (D_2 = 1.1%). The Z1, Z3 and Z4 groups do not form statistically significant peaks in the RPD diagram (Fig. 7d).

Since the youngest detrital zircon grains (group Z1) have statistically irrelevant ages (481 Ma and 509 Ma) and contradict the geological configuration in the region, they should not be applied to estimate a maximum depositional age of the host rocks. Among the studied dZr, we used five grains that were younger than 535 Ma (Fig. 8b) for which all three age estimates were concordant within a 1σ error (Fig. 8a) and $|D_{1 and 2}|$ < 5 to constrain the MDA (maximum depositional age) of the host strata. The calculated concordia and weighted mean $^{206}Pb/^{238}U$ ages for these grains are very close: 531.1 ± 5.2 Ma (MSWD, 0.70; probability, 0.40) and 530.6 ± 5.3 Ma (MSWD, 0.34; probability, 0.85) (Fig. 7c).

5. Discussion

5.a. Age of the Moty Group

The documented small skeletal fossils provide a low degree of certainty regarding the age of the Moty Group of the Irkutsk

Cis–Sayans Uplift. Morphologically primitive tubular *Cambrotubulus*, which are abundant in the Fortunian and are typical of the basal Cambrian Siberian *Anabarites trisulcatus* SSF zone, first appear in the terminal Ediacaran strata (Khomentovsky & Karlova, 1993; Nagovitsin *et al.* 2015; Zhu *et al.* 2017).

The dolostones of the lower Irkut Formation include abundant horizontal burrows, including those putatively produced by priapulids (*Treptichnus*) and arthropods (*Monomorphichnus*), and only scarce simple vertical shafts (*Skolithos*). Only thin intervals of the trace fossil-bearing beds are bioturbated, whereas most of the bed volume reveals undisrupted original sedimentary structures. The ichnotaxonomic composition and stratigraphic distribution of the trace fossils in the upper Irkut Formation are consistent with Fortunian ichnoassemblages (Mángano & Buatois, 2014, 2017). The later stages of the behavioural evolution of endobenthos (younger than *c.* 530 Ma) reveal the development of complex burrowing principles (e.g. spreiten burrows), wide distributions of vertical shafts, and associated prominent increases in bioturbation depths and densities (Mángano & Buatois, 2014; McIlroy & Brasier, 2016; Gougeon *et al.* 2018), which are undocumented in the Moty Group.

The lack or scarcity of trace fossils similar to those documented in the lower Irkut Formation in the underlying strata is putatively attributed to environmental conditions and sedimentary regimes that were unfavourable for Terreneuvian endobenthos: mud and mixed flat and alluvial–deltaic settings. This assumption is
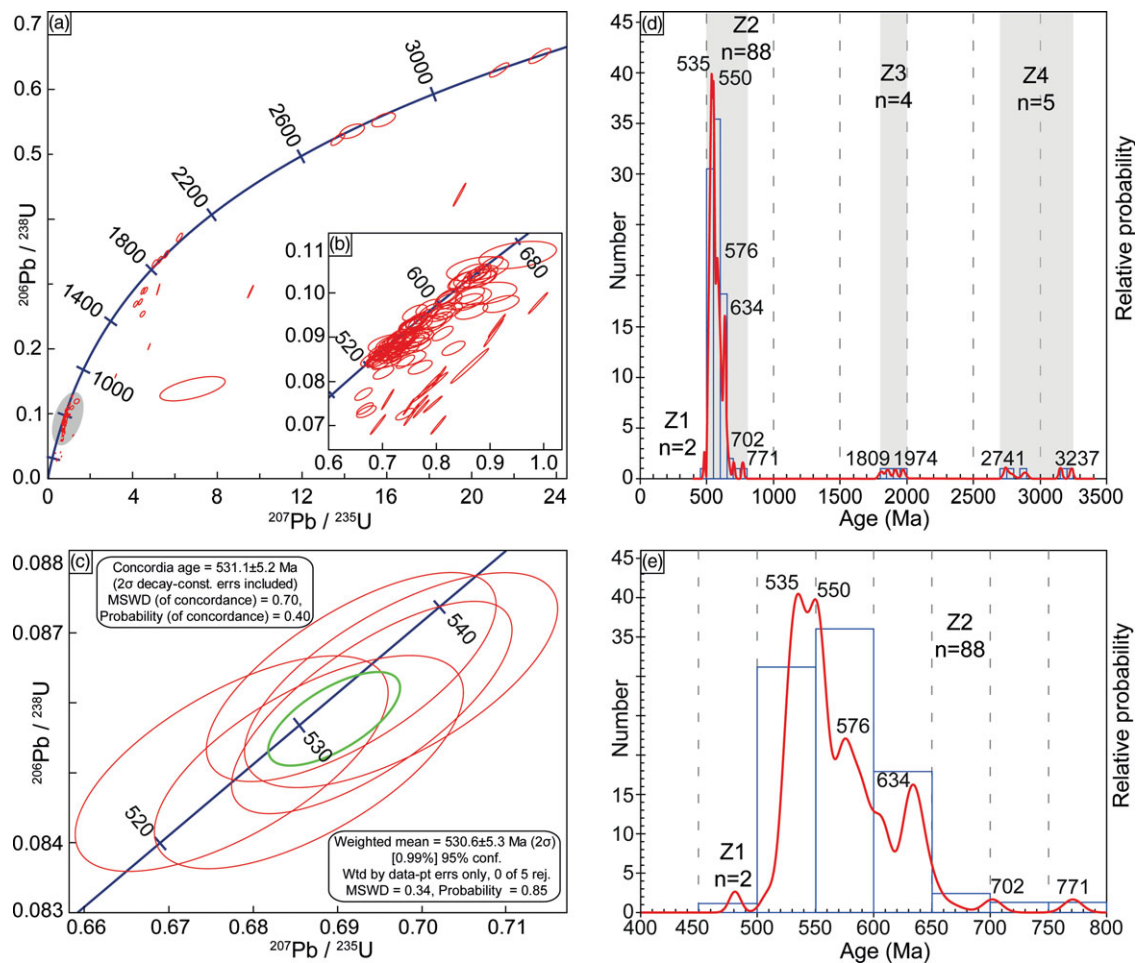
Fig. 7. (Colour online) Plots of LA-ICP-MS U–Pb dating of detrital zircon grains from sample K18-106 (lower Irkut Formation, 28 m above the base; online Supplementary Table S2). (a) Concordia diagram for all 149 U–Pb analyses. (b) Detailed portion of the concordia plot between 480 and 680 Ma, marked with grey in (a). (c) Portion of the concordia plot (a) between 520 and 540 Ma with 1σ ellipses of the five youngest concordant zircon grains (Fig. 8), used for the MDA estimate (both concordia and weighted mean ages are given). The U–Pb concordia age of 531.1 ± 5.2 Ma (2σ) of these grains is shown by the green ellipse. (d) Age spectrum and RPD diagram for detrital zircons from sample K18-106. (e) Detailed portion of the age spectrum and RPD diagram (d) for the Z1 and Z2 zircon groups. MDA – maximum depositional age.

supported by a facies-distribution analysis of *Treptichnus pedum* in the lower Fortunian strata (Buatois *et al.* 2013; Buatois, 2017) and by statistical analyses of the colonization rates of continental and marine environments by burrowing bilaterians (Buatois *et al.* 2005, 2020; Minter *et al.* 2016, 2017). The delayed colonization of the shoreface environments by burrowing organisms, as opposed to offshore environments, also explains the moderate bioturbation and lack of typical Cambrian Stage 2 complex tunnels and spreiten burrows in the lower Irkut Formation when considering the U–Pb concordia age of 531.1 ± 5.2 Ma (weighted mean, 530.6 ± 5.3 Ma) of detrital zircons from the host strata. We presume that the absence of trace fossils in the dolostones of the upper Irkut and lower Usol'e formations was caused by a minimal lithological contrast of the host strata (as well as burrow–host sediment contrasts) and a lack of sand-sized siliciclastic material, which prevented preservation of ichnofabrics and individual burrows during diagenetic recrystallization of the host carbonate sediments.

As noted in Section 2, a previous study of the Moty Group (Sovetov, 2018) suggested a Fortunian age for the upper Shaman Formation and overlying strata based on a similar ichnoassemblage composition of this unit and in the Ust'–Tagul Formation of the Biryusa Cis–Sayans Uplift. The latter does exhibit a typical Fortunian assemblage (Sovetov & Jensen, 2010; Sovetov, 2018, fig. 3b). However, the structures from the upper Shaman Formation, which were previously interpreted as *Treptichnus pedum*, cannot be undisputedly assigned to this ichnospecies (see Section 4a). Since the oldest treptichnids are known from the terminal Ediacaran (Jensen *et al.* 2000; Mángano & Buatois, 2014), the *Treptichnus* isp. from the upper Shaman Formation do not necessitate a Fortunian age for the host and overlying strata.

The Ediacaran–Cambrian transitional interval is characterized by considerable δ13C variations in carbonates between negative (exceeding –6‰) and positive values (up to 7‰) (e.g. Maloof *et al.* 2010; Peng *et al.* 2012; Smith *et al.* 2016). Considering the carbon isotope data separately, the recorded shift from mainly positive δ13C values (up to 3.1‰) in the lower Irkut Formation to negative values (reaching –4.3‰) in its upper part and in the lower Usol'e Formation matches the analogues throughout the entire terminal Ediacaran and Terreneuvian carbon isotope record. The composite carbon isotope curve reveals similar transitions, such as: the late Ediacaran positive carbon isotope plateau (EPIP) (Grotzinger *et al.* 1995; Boggiani *et al.* 2010; Zhu *et al.* 2017; Linnemann *et al.* 2019) and basal Cambrian negative δ13C excursion (BACE) (Zhu *et al.* 2006; Bowring *et al.* 2007; Landing *et al.* 2013); any of the positive (2p-3p-4p; Maloof *et al.* 2010) to negative peaks in the Fortunian; and the transition from
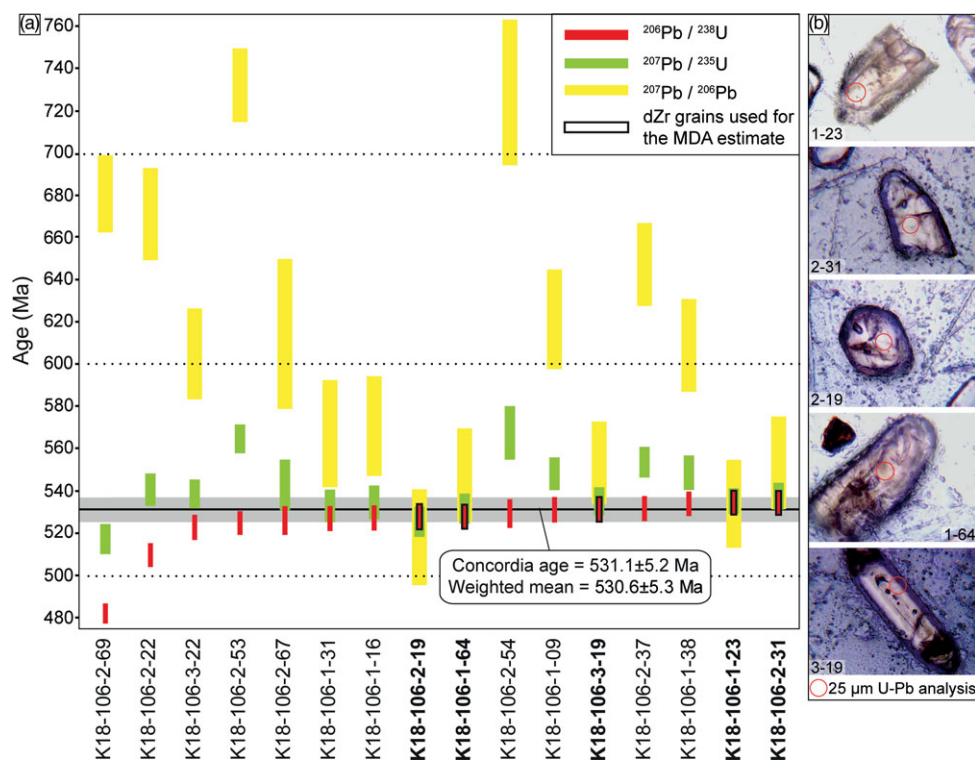
Fig. 8. (Colour online) (a) Correlation of $^{206}Pb/^{238}U$, $^{207}Pb/^{235}U$ and $^{207}Pb/^{206}Pb$ age estimates for the youngest detrital zircons from sample K18-106. (b) Stacked series of optical plane-polarized images of the five youngest concordant detrital zircons used for the MDA estimate (Fig. 7c). MDA – maximum depositional age.

the prominent basal Cambrian Stage 2 positive carbon isotope excursion to the following negative values (SHICE or Shiyantou carbon isotope excursion) (Peng *et al.* 2012; Wood *et al.* 2019). The overall morphology of these carbon isotope anomalies (short peaks versus extensive plateaus) depends highly on sedimentation rates and depositional histories of every particular section on which the composite curve is based. Hence, the shapes of these excursions themselves do not provide evidence that corresponds to the carbon isotope record of the Moty Group.

The U–Pb ages obtained for the five youngest detrital zircon grains from the lower Irkut Formation suggest that the host rocks are younger than 530 Ma (Fig. 6). In this case, the positive $\delta^{13}C$ values correspond to the basal Cambrian Stage 2 excursion. In the composite curve, this excursion (*c.* 529–525 Ma) is named ZHUCE (Zhujiaqing carbon isotope excursion) since it was originally recorded in the Dahai Member of the Zhujiaqing Formation (Yunnan Province, South China) (e.g. Zhu *et al.* 2006; Peng *et al.* 2012). In some sections (e.g. Morocco, northwestern Siberian Platform and Mongolia), however, the lower Cambrian Stage 2 strata are characterized by two distinct positive excursions (in stratigraphic order, 5p and 6p) (Kouchinsky *et al.* 2007; Maloof *et al.* 2010, Smith *et al.* 2016). Any correlation between these two and ZHUCE is controversial (e.g. Marusin *et al.* 2019 for discussion). First, the South China sections do not exhibit any evidence of a second positive excursion above the base of the Cambrian Stage 2 before a shift to negative values (e.g. Li *et al.* 2013). Second, some age estimates of ZHUCE excursion localize it at *c.* 527–526 Ma (Tsukui *et al.* 2017), whereas the first Cambrian Stage 2 index skeletal fossils (*Aldanella attleborensis* and *Watsonella crosbyi*) occur in rocks with positive $\delta^{13}C$ values but as early as 530 Ma (Grazhdankin *et al.* 2020). The data from the Irkutsk Cis–Sayans Uplift do not provide undisputed evidence regarding which of the lower Cambrian Stage 2 excursions (5p, 6p, ZHUCE) corresponds to the excursion in the lower Irkut

Formation. However, the positive-to-negative $\delta^{13}C$ shift in the middle Irkut Formation that follows a negative plateau (Fig. 6) most likely corresponds to a similar change near the top of ZHUCE in South China and 6p in Siberia, Mongolia and Morocco (Maloof *et al.* 2010).

The integrated palaeontological, carbon isotope and geochronological data provide solid evidence for accumulation of the Irkut Formation no earlier than *c.* 530 Ma. Our data provide no evidence for the age of the underlying alluvial to deltaic siliciclastic Shaman and Khuzhir formations. The lower Cambrian boundary commonly lies near or corresponds to an unconformity or sequence boundary (the so-called 'Great Unconformity'; e.g. Peters & Gaines, 2012), which precedes the accumulation of marine deposits during the 'Lower Cambrian transgression'. The unconformity at the base of the Khuzhir Formation (Fig. 1b, d) is therefore one of the levels, and the Cambrian boundary may correspond to the unconformity in the Irkutsk Cis–Sayans Uplift. However, recent detailed evaluations of the stratigraphic completeness of key Ediacaran–Cambrian successions show significant diachronism of the unconformity (in many cases, the boundary occurs within continuous transgressive or highstand successions), which resulted from the interplay of eustasy and local tectonics for each particular basin (Shahkarami *et al.* 2020). Alternatively, the Cambrian boundary may be somewhere in the Shaman Formation. This assumption is indirectly supported by data from boreholes in the Irkutsk Amphitheatre, where deposits underlying the Usol'e Formation reach at least 300 m in thickness and are known as the Moty Formation (Vinogradov *et al.* 2006). These deposits share similar lithological trends with the Irkutsk Cis–Sayans Uplift section. The lower parts of the sections (e.g. lower–middle Moty Formation in the Irkutsk Amphitheatre and the Shaman Formation in the Irkutsk Cis–Sayans Uplift) are transgressive, whereas the upper parts (upper Moty – lower Usol'e, and upper Irkut – lower Usol'e

transitions) are regressive. The lithological disparity of this unit and the siliciclastic Shaman Formation of the Irkutsk Cis–Sayans Uplift putatively mirror the spatiotemporal distributions of facies as a result of changes in sedimentary regime, and are coherent with global trends in early Cambrian facies distributions for the Siberian Platform according to Rozanov (1992) and Sukhov et al. (2016). These authors correlated negative $\delta^{13}C$ values (reaching −6‰) in the carbonate middle Moty Formation (250–300 m) with the BACE excursion (Vinogradov et al. 2006). However, with no additional data currently available (e.g. biostratigraphic data and/or detrital zircon ages), the documented negative excursion alternatively corresponds to any of those in the Fortunian carbon isotope record (e.g. Kouchinsky et al. 2007; Maloof et al. 2010).

Both of these alternatives are speculative because the Shaman and Khuzhir formations consist of alluvial to deltaic successions and therefore present minimal potential for further bio- and chemostratigraphic studies. Detrital zircon geochronology becomes the only tool that can potentially shed light on the location of the Ediacaran–Cambrian boundary within the Moty Group. In its present state, the lower Cambrian boundary may correspond to any level between the Olkha and Irkut formations, and is not mirrored in the palaeontological and carbon isotope records.

5.b. Tectonic settings of the southwestern Siberian Platform during late Ediacaran and Terreneuvian time

Although the lithology of the upper Ediacaran and lower Cambrian strata varies among the regions of the Siberian Platform (e.g. carbonates in the central area and SW with mixed carbonate-siliciclastic sequences in the NE and alongside the SW margin) (Sukhov et al. 2016), all sequences reflect accumulation during eustatic sea-level rise (e.g. Peng et al. 2012). Changes in lithology from the central to northeastern Siberian Platform mirror the transition from subtidal–intertidal and/or lagoonal environments to the open-marine settings of the passive margin (e.g. Rozanov, 1992; Khomentovsky & Karlova, 1993; Pelechaty et al. 1996), although evidence of local rifting and related magmatism is documented for the Olenek and Kharaulakh regions of the northeastern Siberian Platform (Pelechaty et al. 1996; Grazhdankin et al. 2020).

In contrast, the accumulation of thick Ediacaran–Cambrian carbonate-siliciclastic successions along the southwestern margin of the platform (southern Yenisei Ridge, Biryusa Cis–Sayans Uplift, Irkutsk Cis–Sayans Uplift and Cis–Baikal region) reflects filling of the accommodation space of the foreland basin during sea-level rise (Sovetov, 2002, 2018). This foreland basin was formed during early Ediacaran time by multistage accretion of terranes and island arcs at the southwestern margin of the Siberian Platform (e.g. Vernikovsky et al. 2009; Gladkochub et al. 2013; Letnikova et al. 2013; Priyatkina et al. 2018). It was suggested previously that these terranes are (from west to east) the Predivinsk (Vernikovsky et al. 2009), Kan/Arzybey, Tuva–Mongolia, Shaman and Baikal–Muya blocks (Gladkochub et al. 2019). Distinct (or even dominant) Neoproterozoic age clusters of detrital zircons from the Ediacaran–Cambrian sandstones of the southern Yenisei Ridge (Redkolesnaya Formation; Priyatkina et al. 2018), Biryusa Cis–Sayans Uplift (Ust'–Tagul Formation; Priyatkina et al. 2018) and Cis–Baikal region (Ushakovka Formation; Gladkochub et al. 2013) suggest that these terranes and island arcs, along with the Siberian Platform, were the main sources of clastic material that accumulated in the foreland basin. The generally NE-directed

palaeocurrents that were reconstructed for these formations indicate that the source rocks were mostly on the southwestern and southern periphery of the palaeobasin and outside the platform (Sovetov, 2002; Priyatkina et al. 2018). The dominant 'non-Siberian' Neoproterozoic detrital zircon grains (Z1 group) and only accessory Palaeoproterozoic zircons from the Siberian Platform (Z2–Z4 groups) in the Irkut Formation of the Irkut Cis–Sayans Uplift (Fig. 7d) support this suggestion. The accretion of different blocks on the southwestern and southern margins of the platform is mirrored in variations in the compositions of the siliciclastic rocks filling the foreland basin, and is suggested as the main cause of the variations in the accommodation space, the sedimentation rates and hence the thickness of the upper Ediacaran and lower Cambrian siliciclastic strata (350 m, southern Yenisei Ridge; 150 m, Biryusa Cis–Sayans Uplift; 450 m, Irkutsk Cis–Sayans Uplift; and c. 1 km, southwestern Cis–Baikal Region) among the discussed sections (Fig. 3; Sovetov, 2018; Gladkochub et al. 2019). However, since at least c. 530 Ma, all of these sections exhibit more or less similar compositions (shallow-marine carbonates) and reveal no evidence of active tectonics (Sovetov, 2002; Vernikovsky et al. 2009; Sukhov et al. 2016). Hence, the transition from mostly siliciclastic Ediacaran–Cambrian strata to shallow-marine Cambrian carbonates that is observed in all sections along the southwestern margin of the Siberian Platform mirrors the final stages of filling of the foreland basin and the further development of shallow epicontinental marine settings (Sovetov, 2002, 2018).

As was briefly discussed in Section 2, regional correlation commonly plays the major role in age calibrations of the terminal Ediacaran and lower Cambrian transitional strata of the southwestern Siberian Platform. However, scarce palaeontological and unequivocal carbon isotope records often mean that this approach is substantiated only by lithology and facies distributions. Among the units discussed, the salt-bearing carbonate Usol'e Formation clearly illustrates this dilemma. In the ratified correlation schemes and most regional studies (e.g. Krasnov et al. 1983; Shenfil', 1991; Sukhov et al. 2016), this formation is ubiquitously correlated with the Tommotian Stage of the General Stratigraphic Scale of Russia (sensu stricto, upper part of the Cambrian Stage 2) across the entire southwestern Siberian Platform (> 1×10^6 km²). The brecciated dolostones and salt beds, which are treated as regional markers of the basal Usol'e Formation, sporadically occur as thin interbeds within the underlying shallow-marine carbonates, as is seen in the studied section (Fig. 2c) and, moving northwards, in the Tetere–Usol'e transitional interval of the Angara–Nepa region (Melnikov et al. 2005). The similar compositions of the underlying deposits therefore cause precise identification of the lower boundary of the Usol'e Formation to be highly controversial.

Our data support some earlier studies (Kochnev et al. 2018; Marusin et al. 2019) demonstrating that, in at least some regions of the central and southwestern Siberian Platform (Turukhansk–Irkutsk–Olekma facies region), the beginning of Cambrian Stage 2 corresponds to the accumulation of shallow-marine carbonates with no evidence of increased salinity. The salt-bearing lagoonal carbonates, which are ubiquitous within this facies region (Usol'e Formation in the southwestern sections, Bilir Formation in the central sections, and Kostino Formation in the northwestern sections) and have traditionally been regarded as the regional stratigraphic marker (e.g. Krasnov et al. 1983; Sukhov et al. 2016), have a highly diachronous lower boundary, which reflects transgressive–regressive trends and the general palaeorelief of the Siberian Platform during early Cambrian time (i.e. shallowing towards the central part of the platform).

The integrated palaeontological, chemostratigraphic and geochronological study of the Moty Group of the Irkutsk Cis–Sayans Uplift and the summary of age estimates presented for the Ediacaran–Cambrian sections of adjacent areas demonstrate that straightforward lithological correlations potentially cause dramatic misinterpretations of the ages and depositional histories of the strata. Considering the complicated tectonic history of the region and the specific lithological composition of these sections, which are quite unfavourable biostratigraphic methods and limit the application of carbon isotope chemostratigraphy, a combination of geochemical, geochronological and palaeontological methods may be necessary to yield precise age estimates and provide a robust framework for the correlation and further reconstruction of basin evolution.

6. Conclusions

The first appearance of the Cambrian boundary index-ichnotaxon *Treptichnus pedum* at 28 m above the base of the Irkut Formation, shallow bioturbation and overall composition of the associated ichnoassemblage suggest at least a Fortunian age (younger than 541 Ma) for the host strata.

The positive $\delta^{13}C$ excursions in the lower Irkut Formation and U–Pb concordia age of 531.1 ± 5.2 Ma (weighted mean, 530.6 ± 5.3 Ma) obtained from the five youngest detrital grains from the same strata reveal that this unit corresponds to Cambrian Stage 2.

Within the Irkutsk Cis–Sayans Uplift, the base of the Cambrian System putatively corresponds to the unconformity at the base of the Khuzhir Formation or lies somewhere within the alluvial to deltaic Khuzhir and Shaman formations, and is not mirrored in the palaeontological and isotope record. The lack of typical Fortunian trace fossils in the siliciclastic Shaman Formation supports the suggestions that the alluvial-deltaic and intertidal marine settings remained barely occupied by burrowing bilaterians before c. 530 Ma.

References

Andersen T (2005) Detrital zircons as tracers of sedimentary provenance: limiting conditions from statistics and numerical simulation. *Chemical Geology* **216**, 249–70.

Astashkin VA, Pegel TV, Shabanov YY, Sukhov SS, Sundukov VM, Repina LN, Rozanov AY and Zhuravlev AY (1991) *The Cambrian System on the Siberian Platform: Correlation Chart and Explanatory notes*. Herdon: International Union of Geological Sciences, Publication 27, 133 pp.

Babcock LE, Peng S, Zhu M, Xiao S and Ahlberg P (2014) Proposed reassessment of the Cambrian GSSP. *Journal of African Earth Sciences* **98**, 3–10.

Boggiani PC, Gaucher C, Sial AN, Babinski M, Simon CM, Riccomini C, Ferreira VP and Fairchild TR (2010) Chemostratigraphy of the Tamengo Formation (Corumbá Group, Brazil): a contribution to the calibration of the Ediacaran carbon-isotope curve. *Precambrian Research* **182**, 382–401.

Bowring SA, Grotzinger JP, Condon DJ, Ramezani J, Newall MJ and Allen PA (2007) Geochronologic constraints on the chronostratigraphic framework of the Neoproterozoic Huqf Supergroup, Sultanate of Oman. *American Journal of Science* **307**, 1097–145.

Brasier M, Cowie J and Taylor M (1994) Decision on the Precambrian–Cambrian boundary stratotype. *Episodes* **17**, 3–9.

Brasier MD, Khomentovsky VV and Corfield RM (1993) Stable isotopic calibration of the earliest skeletal fossil assemblages in eastern Siberia (Precambrian-Cambrian boundary). *Terra Nova* **5**, 225–32.

Buatois LA (2017) *Treptichnus pedum* and the Ediacaran–Cambrian boundary: significance and caveats. *Geological Magazine* **155**, 174–80.

Buatois LA, Almond J and Germs GJB (2013) Environmental tolerance and range offset of *Treptichnus pedum*: implications for the recognition of the Ediacaran-Cambrian boundary. *Geology* **41**, 519–22.

Buatois LA, Gingras MK, MacEachern J, Mángano MG, Zonneveld J-P, Pemberton SG, Netto RG and Martin A (2005) Colonization of brackish-water systems through time: evidence from the trace-fossil record. *PALAIOS* **20**, 321–47.

Buatois LA, Mángano MG, Minter NJ, Zhou K, Wisshak M, Wilson MA and Olea RA (2020) Quantifying ecospace utilization and ecosystem engineering during the early Phanerozoic – The role of bioturbation and bioerosion. *Science Advances* **6**, eabb0618.

Chechel' EI (1976) A find of *Cyclomedusa* in the Ostrov Formation deposits of the Enisey Ridge. *Geologiya i Geofizika* **17**, 118–20 [in Russian].

Dickinson WR and Gehrels GE (2009) Use of U–Pb ages of detrital zircons to infer maximum depositional ages of strata: a test against a Colorado Plateau Mesozoic database. *Earth and Planetary Science Letters* **288**, 115–25.

Elhlou S, Belousova E, Griffin WL, Pearson NJ and Riley SY (2006) Trace element and isotopic composition of GJ-red zircon standard by laser ablation. *Geochimica et Cosmochimica Acta* **70**, A158.

Erwin DH and Valentine JW (2013) *The Cambrian Explosion: The Construction of Animal Biodiversity*. Englewood: Roberts and Company Publishers Inc., 416 pp.

Fisher RA and Yates F (1974) *Statistical Tables for Biological, Agricultural and Medical Research,* 6th Ed. London: Longman, 156 pp.

Friedman I, O'Neil J and Cebula G (1982) Two new carbonate stable isotope standards. *Geostandards Newsletter* **6**, 11–2.

Gehrels G (2012) Detrital zircon U–Pb geochronology: current methods and new opportunities. In *Tectonics of Sedimentary Basins* (eds C Busby and A Azor), pp. 47–62. Hoboken, New Jersey: John Wiley & Sons.

Gehrels GE, Valencia VA and Ruiz J (2008) Enhanced precision, accuracy, efficiency, and spatial resolution of U-Pb ages by laser ablation–multicollector-inductively coupled plasma mass spectrometry. *Geochemistry, Geophysics, Geosystems* **9**, Q03017.

Gladkochub DP, Donskaya TV, Stanevich AM, Pisarevsky SA, Zhang S, Motova ZL, Mazukabzov AM and Li H (2019) U–Pb detrital zircon geochronology and provenance of Neoproterozoic sedimentary rocks in southern Siberia: new insights into breakup of Rodinia and opening of Paleo-Asian Ocean. *Gondwana Research* **65**, 1–16.

Gladkochub DP, Stanevich AM, Mazukabzov AM, Donskaya TV, Pisarevsky SA, Nicoll G, Motova ZL and Kornilova TA (2013) Early evolution of the Paleoasian ocean: LA-ICP-MS dating of detrital zircon from Late Precambrian sequences of the southern margin of the Siberian craton. *Russian Geology and Geophysics* **54**, 1150–163.

Gougeon RC, Mángano MG, Buatois LA, Narbonne GM and Laing BA (2018) Early Cambrian origin of the shelf sediment mixed layer. *Nature Communications* **9**, 1909.

Grazhdankin DV, Kontorovich AE, Kontorovich VA, Saraev SV, Filippov YF, Efimov AS, Karlova GA, Kochnev BB, Nagovitsin KE, Terleev AA and Fedyanin GO (2015) Vendian of the Fore-Yenisei sedimentary basin (southeastern West Siberia). *Russian Geology and Geophysics* **56**, 560–72.

Grazhdankin DV, Marusin VV, Izokh OP, Karlova GA, Kochnev BB, Markov GE, Nagovitsin KE, Sarsembaev Z, Peek S, Cui H and Kaufman AJ (2020) Quo vadis, Tommotian? *Geological Magazine* **157**, 22–34.

Griffin WL, Powell WJ, Pearson NJ and O'Reilly SY (2008) GLITTER: Data reduction software for laser ablation ICP-MS. In *Laser Ablation ICP-MS in the Earth Sciences: Current Practices and Outstanding Issues* (ed. PJ Sylvester), pp. 308–11. Quebec: Mineralogical Association of Canada, Short Course Series no. 40.

Grotzinger JP, Bowring SA, Saylor BZ and Kaufman AJ (1995) Biostratigraphic and geochronologic constraints on early animal evolution. *Science* **270**, 598–604.

Hantsoo KG, Kaufman AJ, Cui H, Plummer RE and Narbonne GM (2018) Effects of bioturbation on carbon and sulfur cycling across the Ediacaran-Cambrian transition at the GSSP in Newfoundland, Canada. *Canadian Journal of Earth Sciences* **55**, 1240–52.

Horstwood MSA, Košler J, Gehrels G, Jackson SE, McLean NM, Paton C, Pearson NJ, Sircombe K, Sylvester P, Vermeesch P, Bowring JF, Condon DJ and Schoene B (2016) Community-derived standards for LA-ICP-MS U-(Th-)Pb geochronology – uncertainty propagation, age interpretation and data reporting. *Geostandards and Geoanalytical Research* **40**, 311–32.

Jackson SE, Pearson NJ, Griffin WL and Belousova EA (2004) The application of laser ablation-inductively coupled plasma-mass spectrometry to in situ U–Pb zircon geochronology. *Chemical Geology* **211**, 47–69.

Jensen S (1997) Trace fossils from the Lower Cambrian Mickwitzia sandstone, south-central Sweden. *Fossils and Strata* **42**, 110.

Jensen S (2003) The Proterozoic and earliest Cambrian trace fossil record; patterns, problems and perspectives. *Integrative and Comparative Biology* **43**, 219–28.

Jensen S, Saylor BZ, Gehling JG and Germs GJB (2000) Complex trace fossils from the terminal Proterozoic of Namibia. *Geology* **28**, 143–6.

Kaufman AJ and Knoll AH (1995) Neoproterozoic variations in the C-isotopic composition of seawater: stratigraphic and biogeochemical implications. *Precambrian Research* **72**, 27–49.

Kaufman AJ, Knoll AH, Semikhatov MA, Grotzinger JP, Jacobsen SB and Adams W (1996) Integrated chronostratigraphy of Proterozoic-Cambrian boundary beds in the western Anabar region, northern Siberia. *Geological Magazine* **133**, 509–33.

Khomentovsky VV, Faizulin MS and Karlova GA (1998a) The Nemakit-Daldynian Stage of Vendian in the southwestern Siberian Platform. *Doklady Earth Sciences* **363**, 1075–7.

Khomentovsky VV, Fedorov AB and Karlova GA (1998b) The Lower Cambrian boundary in inner areas of the north Siberian Platform. *Stratigraphy and Geological Correlation* **6**, 3–9.

Khomentovsky VV and Karlova GA (1993) Biostratigraphy of the Vendian-Cambrian beds and the lower Cambrian boundary in Siberia. *Geological Magazine* **130**, 29–45.

Khomentovsky VV and Karlova GA (2002) The boundary between Nemakit-Daldynian and Tommotian Stages (Vendian–Cambrian Systems) of Siberia. *Stratigraphy and Geological Correlation* **10**, 217–38.

Khomentovsky VV and Karlova GA (2005) The Tommotian Stage base as the Cambrian lower boundary in Siberia. *Stratigraphy and Geological Correlation* **13**, 21–34.

Khomentovsky VV, Shenfil' VY, Yakshin MS and Butakov EP (1972) *Base Sections of Upper Precambrian and Lower Cambrian Deposits of the Siberian Platform*. Nauka: Moscow, 356 pp. [in Russian].

Kochnev BB and Karlova GA (2010) New data on biostratigraphy of the Vendian Nemakit-Daldynian Stage in the southern Siberian Platform. *Stratigraphy and Geological Correlation* **18**, 492–504.

Kochnev BB, Pokrovsky BG, Kuznetsov AB and Marusin VV (2018) C- and Sr- isotope chemostratigraphy of Vendian-Lower Cambrian carbonates of central Siberian Platform. *Russian Geology and Geophysics* **59**, 585–605.

Kouchinsky A, Bengtson S, Pavlov V, Runnegar B, Torssander P, Young E and Ziegler K (2007) Carbon isotope stratigraphy of the Precambrian-Cambrian Sukharikha River section, northwestern Siberian platform. *Geological Magazine* **144**, 609–18.

Kouchinsky A, Bengtson S, Runnegar B, Skovsted C, Steiner M and Vendrasco M (2012) Chronology of early Cambrian biomineralization. *Geological Magazine* **149**, 221–51.

Krasnov VI, Savitsky VE, Tesakov YI and Khomentovsky VV (eds) (1983) *Resolution of the USSR Stratigraphic Conference on the Precambrian, Palaeozoic and Quaternary Systems of Central Siberia. Part 1. Upper Precambrian. Lower Palaeozoic*. Novosibirsk: SNIIGGiMS, 215 pp. [in Russian].

Landing E, Geyer G, Brasier MD and Bowring SA (2013) Cambrian evolutionary radiation: context, correlation, and chronostratigraphy – overcoming deficiencies of the first appearance datum (FAD) concept. *Earth-Science Reviews* **123**, 133–72.

Lenton TM and Daines SJ (2018) The effects of marine eukaryote evolution on phosphorus, carbon and oxygen cycling across the Proterozoic–Phanerozoic transition. *Emerging Topics in Life Sciences* **2**, 267–78.

Letnikova EF, Kuznetsov AB, Vishnevskaya IA, Veshcheva SV, Proshenkin AI and Geng H (2013) The Vendian passive continental margin in the southern Siberian Craton: geochemical and isotopic (Sr, Sm–Nd) evidence and U–Pb dating of detrital zircons by the LA-ICP-MS method. *Russian Geology and Geophysics* **54**, 1177–94.

Li D, Ling H-F, Shields-Zhou GA, Chen X, Cremonese L, Och L, Thirlwall M and Manning CJ (2013) Carbon and strontium isotope evolution of seawater across the Ediacaran-Cambrian transition: Evidence from the Xiaotan section, NE Yunnan, South China. *Precambrian Research* **225**, 128–47.

Linnemann U, Ovtcharova M, Schaltegger U, Gärtner A, Hauntmann M, Geyer G, Vickers-Rich P, Rich T, Plessen B, Hofmann M, Zieger J, Krause R, Kreisfeld L and Smith J (2019) New high-resolution age data from the Ediacaran-Cambrian boundary indicate rapid, ecologically driven onset of the Cambrian explosion. *Terra Nova* **31**, 49–58.

Liu AG, Brasier MD, Bogolepova OK, Raevskaya EG and Gubanov AP (2013) First report of a newly discovered Ediacaran biota from the Irkineeva Uplift, East Siberia. *Newsletters on Stratigraphy* **46**, 95–110.

Ludwig KR (2012) *User's Manual for Isoplot Version 3.75–4.15: A Geochronological Toolkit for Microsoft Excel*. Berkeley: Berkeley Geochronology Center, Special Publication no. **5**, 75 p.

MacNaughton RB and Narbonne GM (1999) Evolution and ecology of Neoproterozoic-Lower Cambrian trace fossils, NW Canada. *PALAIOS* **14**, 97–115.

Maloof AC, Porter SM, Moore JL, Dudás FÖ, Bowring SA, Higgins JA, Fike DA and Eddy MP (2010) The earliest Cambrian record of animals and ocean geochemical change. *GSA Bulletin* **122**, 1731–74.

Mángano MG and Buatois LA (2014) Decoupling of body-plan diversification and ecological structuring during the Ediacaran-Cambrian transition: evolutionary and geobiological feedbacks. *Proceedings of the Royal Society B* **281**, 20140038.

Mángano MG and Buatois LA (2017) The Cambrian revolutions: trace-fossil record, timing, links and geobiological impact. *Earth-Science Reviews* **173**, 96–108.

Marusin VV, Kochnev BB, Karlova GA and Nagovitsin KE (2019) Resolving Terreneuvian stratigraphy in subtidal-intertidal carbonates: palaeontological and chemostratigraphical evidence from the Turukhansk Uplift, Siberian Platform. *Lethaia* **52**, 464–85.

McIlroy D and Brasier MD (2016) Ichnological evidence for the Cambrian explosion in the Ediacaran to Cambrian succession of Tanafjord, Finnmark, northern Norway. In *Earth System Evolution and Early Life: a Celebration of the Work of Martin Brasier* (eds AT Brasier, D McIlroy and N McLoughlin), pp. 351–68. Geological Society of London, Special Publication no. 448.

Melnikov NV, Yakshin MS, Shishkin BB, Efimov AO, Karlova GA, Kilina LI, Konstantinova LN, Kochnev BB, Kraevskiy BG, Melnikov PN, Nagovitsyn KE, Postnikov AA, Ryabkova LV, Terleev AA and Khabarov EM (2005) *Stratigraphy of Oil and Gas Basins of Siberia. Riphean and Vendian of Siberian Platform and the Adjacent Folded Belts*. Novosibirsk: Academic Publishing House 'Geo', 428 pp. [in Russian].

Minter NJ, Buatois LA, Mángano MG, Davies NS, Gibling MR, MacNaughton RB and Labandeira CC (2017) Early bursts of diversification defined the faunal colonization of land. *Nature Ecology & Evolution* **1**, 0175.

Minter NJ, Buatois LA, Mángano MG, MacNaughton RB, Davies NS and Gibling MR (2016) The prelude to continental invasion. In *The Trace-Fossil Record of Major Evolutionary Events* (eds MG Mángano and LA Buatois), pp. 157–204. Dordrecht: Springer, Topics in Geobiology no. 39.

Moczydłowska M (1991) Acritarch biostratigraphy of the Lower Cambrian and the Precambrian–Cambrian boundary in the southeastern Poland. *Fossils and Strata* **29**, 1–127.

Moczydłowska M (1998) Cambrian acritarchs from Upper Silesia, Poland: biochronology and tectonic implications. *Fossils and Strata* **46**, 1–121.

Nagovitsin KE, Rogov VI, Marusin VV, Karlova GA, Kolesnikov AV, Bykova NV and Grazhdankin DV (2015) Revised Neoproterozoic and Terreneuvian stratigraphy of the Lena-Anabar Basin and northwestern slope of the Olenek Uplift, Siberian Platform. *Precambrian Research* **270**, 226–45.

Nemchin AA and Cawood PA (2005) Discordance of the U–Pb system in detrital zircons: Implication for provenance studies of sedimentary rocks. *Sedimentary Geology* **182**, 143–62.

Nikishin AM, Romanyuk TV, Moskovsky DV, Kuznetsov NB, Kolesnikova AA, Dubensky AS, Sheshukov VS and Lyapunov SM (2020) The Upper Triassic strata of the Mountainous Crimea: the first results of U-Pb dating of detrital zircons. *Moscow University Geology Bulletin* **2**, 18–33.

Pelechaty SM, Grotzinger JP, Kashirtsev VA and Zhernovsky VP (1996) Chemostratigraphic and sequence stratigraphic constraints on Vendian-Cambrian basin dynamics, northeast Siberian Craton. *The Journal of Geology* **104**, 543–63.

Peng S, Babcock LE and Cooper RA (2012) The Cambrian Period. In *The Geologic Time Scale 2012* (eds FM Gradstein, JG Ogg, MD Schmitz and GM Ogg), pp. 437–88. Amsterdam: Elsevier.

Peters SE and Gaines RR (2012) Formation of the Great Unconformity as a trigger for the Cambrian explosion. *Nature* **484**, 363–7.

Pisarchik YK (1963) *Lithology and Facies of Lower and Middle Cambrian Strata of the Irkutsk Amphitheatre in a Context of their Oil- and Salt-Bearing Capability*. Moscow: Gostoptekhizdat, 346 pp. [in Russian].

Pokrovsky BG, Bujakaite MI and Kokin OV (2012) Geochemistry of C, O, and Sr isotopes and chemostratigraphy of Proterozoic rocks in the Northern Yenisei Ridge. *Lithology and Mineral Resources* **47**, 177–99.

Priyatkina N, Collins WJ, Khudoley AK, Letnikova EF and Huang H-Q (2018) The Neoproterozoic evolution of the western Siberian Craton margin: U-Pb-Hf isotopic records of detrital zircons from the Yenisey Ridge and the Prisayan Uplift. *Precambrian Research* **305**, 197–217.

Romanyuk TV, Kuznetsov NB, Belousova EA, Gorozhanin VM and Gorozhanina EN (2018) Paleotectonic and paleogeographic conditions for the accumulation of the Lower Riphean Ai Formation in the Bashkir Uplift (Southern Urals): the Terranechrone® detrital zircon study. *Geodynamics & Tectonophysics* **9**, 1–37 [in Russian with English abstract].

Rozanov AYu (1992) Some problems concerning the Precambrian–Cambrian transition and the Cambrian faunal radiation. *Journal of the Geological Society, London* **149**, 593–8.

Rozanov AY, Missarzhevsky VV, Volkova NA, Voronova LG, Krylov IN, Keller BM, Korolyuk IK, Lendzion K, Michniak R, Pyhova NG and Sidorov AD (1969) *The Tommotian Stage and the Cambrian Lower Boundary Problem*. Moscow: Nauka, 380 pp. [in Russian].

Rozanov AY, Semikhatov MA, Sokolov BS, Fedonkin MA and Khomentovskii VV (1997) The decision on the Precambrian–Cambrian boundary stratotype: a breakthrough or misleading action? *Stratigraphy and Geological Correlation* **5**, 19–28.

Shahkarami S, Buatois LA, Mángano MG, Hagadorn JW and Almond J (2020) The Ediacaran–Cambrian boundary: evaluating stratigraphic completeness and the Great Unconformity. *Precambrian Research* **345**, 105721.

Shenfil' VY (1991) *The Late Precambrian of the Siberian Platform*. Novosibirsk: Nauka, 184 pp. [in Russian].

Sláma J, Košler J, Condon DJ, Crowley JL, Gerdes A, Hanchar JM, Horstwood MSA, Morris GA, Nasdala L, Norberg N, Schaltegger U, Schoene B, Tubrett MN and Whitehouse MJ (2008) Plešovice zircon — A new natural reference material for U–Pb and Hf isotopic microanalysis. *Chemical Geology* **249**, 1–35.

Smith EF, Macdonald FA, Petach TA, Bold U and Schrag DP (2016) Integrated stratigraphic, geochemical, and paleontological late Ediacaran to early Cambrian records from southwestern Mongolia. *GSA Bulletin* **128**, 442–68.

Sovetov JK (1977) *Upper Precambrian Sandstones of the Southwestern Siberian Platform*. Novosibirsk: Nauka, 295 pp. [in Russian].

Sovetov JK (2002) Vendian foreland basin of the Siberian cratonic margin: Paleopangean accretionary phases. *Russian Journal of Earth Sciences* **4**, 363–87.

Sovetov JK (2018) Sedimentology and stratigraphic correlation of Vendian deposits in the southwestern Siberian Craton: major contribution of an exo-cratonic clastic source to sedimentary systems. *Lithosfera* **18**, 20–45 [in Russian with English abstract].

Sovetov JK and Jensen S (2010) Lower Cambrian boundary in the northwestern Siberian Platform: new paleontological and sedimentological data. In *Geodynamic Evolution of Lithosphere of the Central Asian Foldbelt (From Ocean to Continent)*, vol. 2. Irkutsk: Institute of the Earth's Crust of SB RAS, pp. 87–9 [in Russian].

Sukhov SS, Shabanov YY, Pegel TV, Saraev SV, Filippov YF, Korovnikov IV, Sundukov VM, Fedorov AB, Varlamov AI, Efimov AS, Kontorovich VA and Kontorovich AE (2016) *Stratigraphy of Oil and Gas Basins of Siberia. Cambrian of Siberian Platform. Vol. 1 Stratigraphy*. Novosibirsk: Trofimuk Institute of Petroleum Geology and Geophysics of SB RAS, 497 pp. [in Russian].

Tsukui K, Isozaki Y, Zhu M, Ramezani J, Sato T, Zhang X and Bowring SA (2017) High-precision U-Pb temporal constraints on the Early Cambrian diversification of animal life from eastern Yunnan. In *Proceedings of JpGU–AGU Joint Meeting 2017*, Chiba. Makuhari Messe: Japanese Geoscience Union, BCG09-01.

Vernikovsky VA, Kazansky AY, Matushkin NY, Metelkin DV and Sovetov JK (2009) The geodynamic evolution of the folded framing and the western margin of the Siberian craton in the Neoproterozoic: geological, structural, sedimentological, geochronological, and paleomagnetic data. *Russian Geology and Geophysics* **50**, 380–93.

Vinogradov VI, Belenitskaya GA, Bujakaite MI, Kuleshov VN, Minaeva MA and Pokrovskii BG (2006) Isotopic signatures of deposition and transformation of Lower Cambrian saliferous rocks in the Irkutsk Amphitheatre: Communication 3. Carbon and oxygen isotopic compositions in carbonates. *Lithology and Mineral Resources* **41**, 271–9.

Walter MR, Elphinstone R and Heys GR (1989) Proterozoic and Early Cambrian trace fossils from the Amadeus and Georgina Basins, central Australia. *Alcheringa* **13**, 209–56.

Wiedenbeck M, Allé P, Corfu F, Griffin WL, Meier M, Oberli F, von Quadt A, Roddick JC and Spiegel W (1995) Three natural zircon standards for U–Th–Pb, Lu–Hf, trace-element and REE analyses. *Geostandards Newsletter* **19**, 1–23.

Wiedenbeck M, Hanchar JM, Peck WH, Sylvester P, Valley J, Whitehouse M, Kronz A, Morishita Y, Nasdala L, Fiebig J, Franchi I, Girard J-P, Greenwood RC, Hinton R, Kita N, Mason PRD, Norman M, Ogasawara M, Piccoli PM, Rhede D, Satoh H, Schulz-Dobrick B, Skår Ø, Spicuzza MJ, Terada K, Tindle A, Togashi S, Vennemann T, Xie Q and Zheng Y-F (2004) Further characterisation of the 91500 zircon crystal. *Geostandards and Geoanalytical Research* **28**, 9–39.

Wood R, Liu AG, Bowyer F, Wilby PR, Dunn FS, Kenchington CG, Cuthill JFH, Mitchell EG and Penny A (2019) Integrated records of environmental change and evolution challenge the Cambrian Explosion. *Nature Ecology & Evolution* **3**, 528–38.

Yang B, Steiner M, Li G and Keupp H (2014) Terreneuvian small shelly faunas of East Yunnan (South China) and their biostratigraphic implications. *Palaeogeography, Palaeoclimatology, Palaeoecology* **398**, 28–58.

Yao J, Xiao S, Yin L, Li G and Yuan X (2005) Basal Cambrian microfossils from the Yurtus and Xishanblaq formations (Tarim, North-West China): Systematic revision and biostratigraphic correlation of *Micrhystridium*-like acritarchs. *Palaeontology* **48**, 687–708.

Yuan H-L, Gao S, Dai M-N, Zong C-L, Günther D, Fontaine GH, Liu X-M and Diwu C (2008) Simultaneous determinations of U–Pb

age, Hf isotopes and trace element compositions of zircon by excimer laser-ablation quadrupole and multiple-collector ICP-MS. *Chemical Geology* **247**, 100–18.

Zhu M, Babcock LE and Peng S (2006) Advances in Cambrian stratigraphy and paleontology: integrating correlation techniques, paleobiology, taphonomy and paleoenvironmental reconstruction. *Palaeoworld* **15**, 217–22.

Zhu M, Yang A, Yuan J, Li G, Zhang J, Zhao F, Ahn S-Y and Miao L (2018) Cambrian integrative stratigraphy and timescale of China. *Science China Earth Sciences* **62**, 25–60.

Zhu M, Zhuravlev AY, Wood RA, Zhao F and Sukhov SS (2017) A deep root for the Cambrian explosion: implications of new bio and chemostratigraphy from the Siberian Platform. *Geology* **45**, 459–62.